Ectopic FVIII expression and misfolding in hepatocytes as a potential cause of human hepatocellular carcinoma

Audrey Kapelanski-Lamoureux[2*], Zhouji Chen[1*], Zu-Hua Gao[3,4&], Ruishu Deng[1], Anthoula Lazaris[4], Cynthia Lebeaupin[1], Lisa Giles[5], Jyoti Malhotra[6], Jing Yong[1], Chenhui Zou[8], Ype P. de Jong[8], Peter Metrakos[7], Roland W. Herzog[10], Randal J. Kaufman[1,9#]

1 Degenerative Diseases Program, SBP Medical Discovery Institute, La Jolla, United States

2 Department of Anatomy and Cell Biology, McGill University, Cancer Research Program, Research Institute of the McGill University Health Centre, Montreal, Quebec, Canada

3 Department of Pathology and Oncology, McGill University Health Centre, Montreal, Quebec, Canada

4 Cancer Research Program, Research Institute of the McGill University Health Centre, Montreal, Quebec, Canada

5 Not affiliated with any institution

6 Sarepta Therapeutics, Boston MA, United States

7 Department of Surgery, McGill University; Cancer Research Program, Research Institute of the McGill University Health Centre, Montreal, Quebec, Canada

8 Division of Gastroenterology and Hepatology, Weill Cornell Medicine, New York, NY, United States

9 Department of Pharmacology, University of California, San Diego, La Jolla, United States

10 Herman B Wells Center for Pediatric Research, Indiana University, Indianapolis, IN, United States

***** These authors contributed equally to this work.

& Present Address: Department of Pathology & Laboratory Medicine, University of British Columbia, Vancouver, British Columbia, Canada

Corresponding Author:

Randal J. Kaufman: rkaufman@sbpdiscovery.org

Running title: Expression of FVIII in hepatocytes is carcinogenic

Abstract

Clotting factor VIII (FVIII) is the protein deficient in the bleeding disorder hemophilia A (HA). FVIII is a 330 kDa glycoprotein with a domain structure of A1-A2-B-A3-C1-C2. The B domain is dispensable for activity but *in vivo* hepatocyte transfection with B domain deleted (BDD) DNA vector resulted in FVIII misfolding, endoplasmic reticulum (ER) stress, and apoptosis in murine hepatocytes. In addition, mice exposed to transient ER stress through expression of a different misfolded protein and then fed a diet (HFD) for 9 months developed hepatocellular carcinoma (HCC). Therefore, we tested whether ectopic expression of BDD followed by HFD feeding may also cause HCC. Here we compared two FVIII variants with different folding efficiencies in the ER upon expression in hepatocytes in mice: 1) BDD; and 2) N6 which retains 226 amino acids from the B domain with 6 N-linked glycans that does not significantly aggregate or cause hepatocyte apoptosis. We directed transient expression of BDD or N6 from a DNA vector in hepatocytes of 6-week-old mice. One week later, mice were fed 60% HFD for 65 weeks. Remarkably, 100% of mice that received BDD vector developed liver tumors, whereas only 58% of mice that received N6 vector and none of the mice that received empty vector developed liver tumors. The findings suggest that increased protein misfolding in the ER can predispose to HCC in the context of a HFD. They also raise attention regarding the safety of ectopic expression of BDD in hepatocytes during FVIII gene therapy in humans.

Key points:

Expression of BDD FVIII in murine hepatocytes *in vivo* causes accumulation of misfolded FVIII aggregates in the endoplasmic reticulum.

Hepatocyte BDD expression with subsequent high-fat diet induces liver tumors that are reduced upon expression of a well-folded FVIII variant.

Introduction

Hemophilia A (HA) is an X chromosome-linked bleeding disorder affecting 24.6 per 100,000 males at birth that results from deficiency of clotting factor VIII (FVIII) (1). Protein replacement therapy with recombinant FVIII has significantly reduced morbidity and mortality associated with HA, although concerns remain. First, anti-FVIII inhibitory antibodies develop in a significant number of patients (2). Second, recombinant FVIII protein bears a high cost with limited availability due to low and variable production from mammalian host cells, primarily Chinese Hamster Ovary (CHO) or baby hamster kidney cells (3). FVIII secretion from mammalian cells is inefficient, partly due to FVIII protein misfolding, aggregation, and retention in the endoplasmic reticulum (ER) (4). Misfolded FVIII activates the unfolded protein response (UPR) to resolve defective protein folding. However, upon chronic protein misfolding in the ER, the UPR shifts to an apoptotic program.

FVIII is a 330 kDa glycoprotein comprised of three domains (A1-A2-B-A3-C1-C2) (5). It is primarily produced by liver sinusoidal endothelial cells (6). The amino acid (aa) sequences in the A and C domains exhibit 40% amino acid homology between species, whereas the ~900 aa sequences within the large B domain show no other homology than a conserved large number (18) of N-linked oligosaccharides that are also observed in the B domains of FVIII from different species, as well as in the homologous clotting factor V. Deletion of the entire B domain (7, 8) in BDD FVIII (A1-A2-A3-C1-C2) (**Fig. 1**) is completely functional and similar to Refacto (i.e., SQ-BDD FVIII; Pfizer), an effective protein replacement therapy for HA patients (9-11). The only difference between BDD and SQ-BDD is that SQ-BDD contains an extra 14 amino acid linker (SFSQNPPVLKRHQR) at the junction between the A2 and A3 domains (12, 13). Subsequent codon optimization improved SQ-BDD production leading to its use in ongoing HA gene therapy clinical studies (12-16). SQ-BDD is used for gene therapy because the size of full-length FVIII is beyond the packaging limit of the AAV genome, which is <5kb (15). However, BDD exhibits similar misfolding as intact FVIII, activates the UPR, and leads to hepatocyte death upon *in vivo* DNA vector delivery to hepatocytes in mice (17). Besides BDD, we described a partial B domain deletion molecule, herein (N6), that retains an additional 226 aa with 6 N-linked glycosylation sites from the N-terminal portion of the B domain (18) (**Fig. 1**), and is secreted ~10-fold more efficiently than full-length FVIII or BDD (17), presumably due to the 6 N-glycans that engage the intracellular lectin chaperone machinery, demonstrated to enhance FVIII trafficking from the ER to the Golgi compartment (19-24). Thus, N6 is secreted more efficiently and causes less toxic cellular responses than BDD (**Fig. 1**).

Detailed studies of full-length human FVIII expression in mammalian cells demonstrated that FVIII forms amyloid-like aggregates in the ER. When FVIII expression reaches a threshold, it aggregates in the ER (25-27). In addition, aggregation was increased upon glucose deprivation. Significantly, upon glucose repletion the FVIII aggregates dissolved and, remarkably, refolded to produce functional secreted FVIII. Our studies revealed that an amino acid sequence motif in the A1 domain was necessary and sufficient to seed β-sheet polymerization of FVIII (26).

Presently, there are numerous ongoing adeno-associated-viral (AAV) directed gene therapy clinical studies to deliver codon-optimized SQ-BDD to hepatocytes in men with severe HA. Initial results appeared to be very successful, with correction of FVIII levels into the normal range during the first year (13, 14). Substantial improvement in hemostasis was documented at a 5-yr follow-up (28). Unfortunately, elevated liver enzyme levels were observed in the first year, and FVIII expression levels gradually declined to the lower end of the therapeutic range, starting in the second year (29-32). Although the cause for the decline in FVIII expression in the clinical setting is unknown, it is possible that FVIII misfolding and UPR activation impact hepatocyte function, health, and/or survival. Therefore, there is an urgent need to understand mechanisms underlying inefficient FVIII secretion both for engineered bio-production, and importantly, for *in vivo* clinical HA gene therapy (29-31).

Hepatocellular carcinoma (HCC) is the most common primary liver cancer and the 3rd leading cause of cancer deaths worldwide (33). The incidence of HCC has tripled since 1980 and is the most increasing cause of cancer mortality in the U.S. (34). While the incidence of viral-related HCC is declining, HCC related to metabolic stress is on the rise, due to the global increase in obesity and the associated metabolic syndrome (35). It is currently estimated that nonalcoholic steatohepatitis (NASH), which is already the leading cause of liver transplants in developed countries, will become the dominant HCC etiology. A quarter of the world's population suffers from non-alcoholic fatty liver disease (NAFLD) characterized by abnormal lipid accumulation in hepatocytes. A subset of NAFLD patients eventually develops NASH with inflammation, hepatocyte ballooning, Mallory Denk Bodies, cell death, fibrosis, cirrhosis, and HCC. Both ER stress and activation of the UPR are documented in many different human diseases (36, 37), including NASH and HCC (38-40).

Previously, we demonstrated that protein misfolding in the ER of hepatocytes in mice can initiate development of NASH and HCC (41). This study used transgenic mice that express plasminogen activator urokinase (uPA) under the control of the major urinary protein (MUP) promoter (*MUP-*

uPA) in hepatocytes. These mice express uPA until 6 wks of age that is subsequently extinguished by 10 wks, presumably due to hepatocyte toxicity of misfolded uPA expression (41). At 10 wks of age the mice were fed a HFD (60% calories from high fat) for 10 mon. Although transgenic and wild-type mice both developed fatty liver disease, only the *MUP-uPA* transgenic mice developed features of NASH similar to humans. All transgenic mice developed HCC that was not observed in wild-type mice without the *MUP-uPA* transgene and fed HFD. Thus, it appears that either transient expression of a misfolded protein in the ER that activates the UPR followed by a HFD can initiate HCC development or there are unique properties of uPA that drive HCC progression. These findings led us to speculate that transient hepatocyte expression of FVIII, which is prone to misfolding, may also cause similar HCC in mice. Since we described two FVIII molecules that exhibit different degrees of misfolding, we were in a unique position to address the relationship between ER protein misfolding and HCC development in mice.

Here we studied the long-term outcome of transient expression of BDD, which aggregates in the cell and activates the UPR, and N6 that displays reduced aggregation and UPR activation. We delivered BDD and N6 expression vectors to the murine liver by tail vein hydrodynamic DNA injection, for which FVIII expression was extinguished after 5 days. These mice were then fed a HFD for 65 wks starting at one wk after vector DNA injection. We observed greater tumor formation in BDD injected mice than N6 injected mice. For the first time these findings support the notion that the degree of ER protein misfolding may be a significant factor in liver disease progression. Our findings demonstrate the potential risk regarding ectopic expression of FVIII in hepatocytes in the context of HA gene therapy.

Results

FVIII forms aggregates that resolve at 1 hr following energy repletion.

Stable expression of BDD and N6 FVIII in CHO cells demonstrated that N6 expression was tolerated at an ~10-fold greater level than BDD. We previously characterized full-length FVIII aggregation by filtration of cell lysates through nitrocellulose (NC) membranes, which retain all cell proteins, or cellulose acetate (CA) membranes, which only retain proteins that have b-sheet aggregate structures (26). Lysate proteins retained on membranes were probed with FVIII or β-actin antibodies. Filtration through NC membranes demonstrated that intracellular levels of BDD were ~10-fold greater than N6, proportional to the higher level of N6 FVIII secretion. Filtration through CA membranes demonstrated significant aggregation of BDD and ~3-fold less aggregation for N6, although N6 was expressed at a ~10-fold greater level than BDD (**Fig. 2A**).

Following energy depletion by treatment with 2-deoxyglucose (2-DG) and sodium azide (NaN_3) to inhibit glycolysis and oxidative phosphorylation, respectively, FVIII aggregates accumulated in CHO cells that stably express wtFVIII (~500mU/ml/10^6 cells/day, not shown) (26), BDD (~1U/ml/10^6 cells/day), and N6 (~10U/ml/10^6 cells/day). We previously demonstrated that 2-DG, but not NaN_3, was sufficient to induce wtFVIII aggregation (26). It is notable that NaN_3 inhibition of oxidative phosphorylation is irreversible. After 2-DG removal and glucose replenishment, BDD and N6 aggregates began to disappear at 1 hr, in a manner that did not require *de novo* protein synthesis as addition of the protein synthesis elongation inhibitor cycloheximide (CHX) did not alter aggregate dissolution or significantly reduce secretion of functional FVIII (**Fig. 2A**).

We performed [^{35}S]-met/cys-pulse-chase labeling which confirmed that glucose deprivation retained BDD and N6 within the cell, and that upon glucose repletion, intracellular aggregated FVIII dissolved and was efficiently secreted into the medium (**Fig. 2B**). Analysis of FVIII activity in the conditioned media from cells treated under the same conditions as the pulse-chase assay demonstrated that the secreted FVIII is functional (**Fig. 2B, aPTT assay**). Increasing amounts of functional FVIII appeared in the media as early as 1 hr following glucose repletion for BDD and at 2 hr for N6, which correlated with the disappearance of intracellular aggregated FVIII. Without affecting the amount of previously metabolically labeled FVIII secreted following glucose repletion, CHX treatment reduced secreted FVIII activity to 30-60%, presumably due to inhibition of new FVIII synthesis. In sum, these results (**Figs. 2A-B**) indicate that a major percent of both BDD and N6 metastable aggregates can resolve to produce folded, functional, and secreted FVIII.

Ectopic FVIII expression in hepatocytes causes protein aggregation in murine livers.

Hydrodynamic tail vein injection of vector DNA is an efficient method to express exogenous genes in hepatocytes (18, 42). Using this technique, we confirmed expression of exogenous FVIII in hepatocytes of mice injected with BDD or N6 vector DNA induced the UPR, although the stress response to N6 expression was significantly attenuated (17). To determine if the stress response from FVIII gene delivery to hepatocytes is associated with protein aggregation *in vivo*, we performed thioflavin-S (Thio-S) staining on the liver sections to specifically stain amyloid-like protein aggregates. The livers of BDD vector-injected mice showed significantly more Thio-S positivity than N6 vector-injected mice, evidenced by colocalization of Thioflavin-S staining with FVIII immunostaining (**Fig. 3**). Similar to BDD expression in CHO cells (26), these findings demonstrate that ectopic expression of BDD in hepatocytes *in vivo* also leads to intracellular accumulation of amyloid-like FVIII aggregates in the liver.

BDD misfolds in murine hepatocytes *in vivo.*

Misfolded proteins bind the ER chaperone BiP/GRP78 while well-folded proteins do not (43, 44). Therefore, protein interaction with BiP can be used as a surrogate to measure ER protein misfolding. However, there are no available antibodies that can quantitatively co-immunoprecipitate (IP) BiP-client protein complexes. Hence, we created a genetically modified mouse with a 3x Flag tag inserted into the endogenous BiP/GRP78/*Hspa5* locus (*BiP-Flag* mice) to allow for quantitative isolation of BiP-client protein complexes using anti-Flag magnetic beads without altering BiP function or BiP expression, which is essential to measure physiological interactions [**Figs. 4A-B**; (45, 46)]. Importantly, hepatocyte-specific BiP-Flag shares the same level of expression and is regulated identically to the endogenous *Hspa5* locus (**Fig. 4B**). To gain further insight into the folding status of BDD and N6 ectopically expressed in murine hepatocytes, we expressed BDD and N6 in livers of *BiP-Flag* homozygous (*BiP-Flag*$^{+/+}$) mice by hydrodynamic delivery of vector DNA and analyzed the interactions between BiP-Flag and BDD or N6 through anti-Flag co-IP of BDD and N6 (**Fig. 4C**). Consistent with our previous observations (17), hepatic BDD levels in BDD vector-injected mice were significantly higher than those in the N6 vector-injected mice (**Fig. 4C**, lanes 21 & 22 vs lanes 23 & 24), probably due to the greater retention of BDD in the ER. Importantly, anti-Flag IP pulled down a significant portion of BDD from the livers of BDD vector-injected *BiP-Flag*$^{+/+}$ mice (**Fig. 4C**, lanes 13-14), while N6 was pulled down at a 70% lesser level (**Fig. 4C**, lanes 13 &14 vs 17 &18). These results support the notion that BDD exhibits greater misfolding than N6 in hepatocytes of murine livers, which may account for the different degrees of UPR induction (17).

Lentiviral transduction of BDD into human primary hepatocytes activates the UPR.

We then used mouse-passaged human primary hepatocytes (mpPHH) (47) to investigate the cellular response to ectopic BDD expression in human hepatocytes. The mpPHH were transduced *in vitro* with increasing amounts of a lentiviral vector that expresses a codon-optimized SQ-BDD cDNA (12) [all current liver-directed HA gene therapy trials utilize codon-optimized SQ-BDD (13, 14, 16)]. Consistent with our findings on BDD expression in CHO cells and livers of mice injected with BDD expression vector DNA (17), Western blot analysis demonstrated SQ-BDD expression induced UPR markers BiP, eIF2α phosphorylation, and CHOP, despite its weak signal, at 10 days after infection (**Fig. 5**). Interestingly, the protein levels of two UPR-induced genes in the liver, hepcidin (48) and cysteine rich with EGF like domains 2 (CRELD2), an oncogene associated with HCC that promotes survival upon ER stress (49-52), were increased

in BDD-expressing mpPHH. These results for the first time show that ectopic BDD expression induces ER stress in human hepatocytes.

HCC development correlates with the degree of ER protein misfolding.

Previous findings suggest protein misfolding in the ER can initiate NASH and HCC development (41); therefore, we tested whether two different FVIII variants that misfold to different degrees can initiate pathways of HCC development. *C57BL/6J* mice were subjected to hydrodynamic injection of empty vector, BDD, or N6 vector DNA (17). After 24 hr, plasma levels of N6 FVIII were significantly higher than those for BDD (**Fig. 6A**), consistent with our previous observations (17). After 1 wk, when FVIII expression was not detectable (which is typical of tail vein DNA delivery to hepatocytes), mice were fed a 60% HFD for 65 wks and then analyzed for liver surface tumors. No tumors, neither adenomas nor adenocarcinomas, were observed in mice that received empty vector DNA. In contrast, all mice that received BDD expression vector developed tumors, while reduced tumor formation was observed in mice that received N6 vector (**Fig. 6B**).

The tumors (both adenomas and carcinomas) in the above mice were evaluated and extensively characterized independently by three clinical pathologists. A detailed summary of this histopathological analysis is provided in **Supplementary Tables I** and **2**. Immunohistochemistry staining of CD34, glutamine synthetase, β-catenin, glypican 3, and CD44 were also performed to assist the diagnosis. Although no tumors were detected in any of the 8 mice injected with empty vector, we observed that 58% (7/12) of mice that received N6 vector developed liver tumors; in contrast to 100% (10/10) of mice delivered with BDD vector (**Fig. 6B**, $p<0.02$, Chi-square test). The findings suggest a higher penetrance of tumors in the presence of BDD misfolded protein. Detailed histopathological assessment of the BDD-injected mice demonstrated that 6 of the 10 lesions were adenomas and 4 carcinomas (**Fig. 6B**), while the N6 vector DNA-injected mice developed 4 adenomas and 3 carcinomas (**Supplemental Fig. 1A**). The adenomas were overall negative for CD34 whereas the carcinomas displayed a patchy strong CD34-positive staining (**Supplemental Fig. 2**), further confirming the malignancy (53, 54). Most carcinomas had positive glutamine synthetase (GS) staining (**Fig. 6C)**, indicative of an early-stage HCC (55). However, a few well-differentiated HCCs and an early evolving HCC, arising from adenomas, were GS negative. As expected, β-catenin immunostaining showed identical results to GS as they are both frequently overexpressed in early HCC (55). Finally, the adenomas in the BDD cohort were positive for CD44, with the sinusoidal lymphocytes staining while the adenomas in the N6 were negative (**Supplemental Fig. 2**). Based on these histopathological assessments, the distribution

of adenomas and carcinomas appears to be similar in both groups (**Fig. 6C**; **Supplemental Fig. 1A**). However, BDD mice developed more tumors and thus a more aggressive phenotype.

Partial retention of the FVIII B domain in N6 reduces BiP protein levels in carcinomas.

Tumor cells among the BDD carcinomas had significantly higher ($p = 0.04$) BiP protein levels compared to N6 carcinomas (**Figs. 7A-7B** & **Supplemental Fig. 3**). Similarly, we observed the same trend comparing distal normal liver BiP signal positivity ($p = 0.01$) (**Fig. 7A**). Tumor cells among the N6 adenomas showed no significant differences in BiP protein levels compared to BDD adenomas (**Fig. 7A & 7C**). However, two of the BDD adenomas had high BiP levels, which skews the positivity to show no significant difference. One of the cases was an inflammatory subtype adenoma and the other a mild steatosis. Therefore, it appears that the transient expression of BDD or N6 may display memory after 65 wks of HFD upon analysis of those tumors. It is possible epigenetic modifications may persist during initiation and progression of HCC, a subject that requires further investigation. It is notable that BiP expression reduces apoptosis, which may account for the higher levels in HCC. Increased BiP expression correlated with malignancy, metastasis, and drug resistance and is associated with a poor prognosis in HCC (56-58).

Discussion

Hepatic gene transfer of codon-optimized SQ-BDD-FVIII cDNA using AAV vectors has emerged as a promising therapeutic approach for HA (13, 14). Substantial improvement in hemostasis was documented at a 5-yr follow-up (28). However, this gene therapy approach has encountered two major hurdles: 1) A requirement for very high vector doses to drive FVIII expression in hepatocytes; and 2) Declining therapeutic transgene expression over time accompanied with signs of liver damage, both of which may be directly linked to the fact that FVIII is retained and prone to misfolding in the ER during therapy (29-32). All recent HA gene therapy clinical studies suggest the expression is not durable, which is a major factor in considering gene therapy for HA as it is safely and effectively treated by prophylaxis with recombinant FVIII as well as FVIII-bypassing molecules such as bispecific antibody (32) raising the safety and efficacy bars for evaluation of HA gene therapy regimens. The high significance of this problem was highlighted in recent editorials (29, 59, 60). Here, we demonstrate the tumorigenic potential for cellular stress resulting from even transient hyper expression of FVIII in hepatocytes. Encouragingly, we find that a better secreted FVIII variant can be developed to reduce this risk. While there are differences in the biology of human and murine HCC and AAV gene transfer differs from plasmid

vectors, these outcomes warrant more extensive investigations on the potential of current gene therapy approaches to cause tumor formation in patients with HA.

It is likely that nearly all approaches to cell/gene therapy for HA will involve overexpression or ectopic expression of FVIII in hepatocytes that do not normally express FVIII and thus it is important to understand the biosynthetic pathway, host factors, and cellular responses to misfolded FVIII. Significantly, we demonstrated that increased FVIII synthesis does not translate to increased FVIII secretion (26). We propose that simply increasing FVIII expression in transduced cells may not be sufficient to overcome the poor durability of HA gene therapy and may even induce potential unwanted off-target and toxic responses. This view is further supported by a recent publication, showing that the overexpression BDD-FVIII in murine hepatocytes from an AAV vector induces the UPR (61), which may be avoided by achieving therapy through limited expression in a high percentage of hepatocytes.

We and others have identified new aspects of hepatocyte function that are impacted by FVIII misfolding in the ER that include: 1) Activation of the ER UPR; and 2) Activation of cell death pathways (17). We here find that when combined with HFD-feeding, transient expression of BDD or N6 FVIII is sufficient to initiate pathways of HCC development. This finding supports the notion that protein misfolding in the ER is sufficient to induce hepatocarcinogenesis, which is very important, especially in the context of gene therapy. HCC may develop in response to repeated rounds of hepatocyte death and proliferation in the cirrhotic liver. Compensatory proliferation might create a permissive environment for the genetic and epigenetic changes to cause oncogene activation and/or loss of function of tumor-suppressor genes (36, 62)**.**

Our previous work identified a FVIII derivative, N6, that is more efficiently secreted and less prone to aggregation than present B-domain deletion molecules being tested for HA gene therapy (17, 18). In addition to the increased secretion efficiency of N6 compared to BDD, N6 elicits reduced cellular toxicity, as measured by UPR activation, apoptosis, levels of reactive oxygen species (ROS), protection by antioxidant BHA treatment, and HCC (**Fig. 1**) (17, 18, 63, 64).

We tested whether expression of BDD or N6 truncated FVIII proteins that cause different degrees of protein misfolding and UPR activation can induce HCC upon subsequently feeding an HFD. In essence, the degree of protein misfolding in the ER correlated with subsequent HCC development. N6 folds and is secreted more efficiently than BDD when expressed in hepatocytes at a similar level. Thus, a higher level of N6 FVIII expression is tolerated by hepatocytes *in vivo*.

This is consistent with analysis of expression of these two molecules in CHO cells (Fig. 2). Using our recently generated *BiP/GRP78/Hspa5*-knockin mice harboring a 3X FLAG tag in the C-terminus of BiP in the endogenous *BiP/GRP78/Hspa5* locus (46) to assess the folding status of BDD accumulated in hepatocytes *in vivo*, we show that nearly half of intrahepatocellular BDD binds BiP (Fig. 3), indicative of misfolding. This finding supports our hypothesis that compared to N6, ectopic expression of BDD induces a higher level of misfolded FVIII in the liver, which can induce a series of cytotoxic responses, including activation of the UPR, and ultimately leading to initiation of HCC development. This *BiP-Flag* mouse model should be incorporated to evaluate the misfolding propensity of any BDD derivatives considered for gene therapy. Moreover, while N6 is not suitable for HA gene therapy due to the large size of its coding sequence, our findings demonstrating the beneficial properties of such FVIII variants over BDD underscore the need for identifying new FVIII molecules for effective and safe HA gene therapy.

Our findings also suggest that characterization of the folding efficiency, host response, and safety in model organisms and non-human primates is essential to ensure safety over the lifetime of an individual, given that HCC takes years to develop in humans. A case of HCC has occurred in a hemophilia B patient after hepatic AAV-mediated factor IX gene transfer (65). In this event, it was unlikely that tumor formation was caused by gene therapy as it occurred early after gene transfer and the patient had multiple risk factors that pre-disposed to HCC. While HCC formation was observed in murine studies with AAV vectors using other transgenes, this was attributed to insertional mutagenesis and the relevance of this observation to the safety of HA gene therapy remains to be understood. However, our new results show that high levels of FVIII gene expression by itself, even if transient and very likely independent of insertional events, can induce HCC in the context of a HFD. All murine models of NASH and HCC progression require a hypercaloric diet, presumably to induce an inflammatory environment (66, 67). HCC has not been observed in animals treated with AAV-FVIII vectors but these animals were not subjected a HFD challenge. Interestingly, HCC only developed upon neonatal gene transfer but not in mice transduced as adults unless they were fed a HFD leading to NAFLD (68), which was associated with increased inflammation and hepatocyte proliferation, consistent with our findings. Nevertheless, it should be considered that our studies do not reflect the course of liver disease in clinical studies, nor the therapeutic approach. For instance, we used DNA delivery in our mouse studies because we previously characterized detailed responses to BDD vs N6 (17). In AAV gene transfer, it is possible that the amount of FVIII produced by hepatocytes does not typically reach a threshold required to set off the cascade of molecular events that promotes HCC. Long-term

follow-up in patients who have high levels of FVIII expression will be required to answer this question.

Our studies also support the need for careful monitoring of liver function over the time course of gene therapy treatment. We demonstrate the role of diet when expressing a therapeutic protein in the liver that is prone to misfolding and ER stress. While AAV-FVIII gene transfer has not been found to cause the level of hepatocyte apoptosis and liver injury that may occur with DNA vectors, multiple studies have shown induction of ER stress markers in mice in response to AAV-FVIII (61, 69, 70), and liver injury (albeit of unknown origin) occurred in patients treated with high-dose AAV-FVIII (13, 14). We have now directly shown that expression of SQ-BDD in primary human hepatocytes induces ER stress in the dose-dependent manner (**Fig. 5**). Together, our study provides experimental evidence demonstrating the need for rigorous scientific investigations towards the pathophysiological consequence upon AAV-mediated FVIII expression in the hepatocytes to improve the efficacy and safety of HA gene therapy.

Materials and Methods

Materials for cellular and molecular biology

Anti-factor VIII heavy chain monoclonal antibody coupled to Sepharose CL-4B was a kind gift from Baxter/Baxalta Corp. FVIII-deficient and normal pooled human plasmas were obtained from George King Biomedical (Overland Park, KS). Activated partial thromboplastin (automated aPTT reagent) and $CaCl_2$ were purchased from General Diagnostics Organon Teknika (Durham, NC). Dulbecco's modified Eagle medium (DMEM), glucose-free DMEM, alpha-modified essential medium (alpha-MEM), cysteine/methionine-free DMEM, and fetal bovine serum (FBS) were purchased from Gibco BRL. FVIII:C-EIA was purchased from Affinity Biologicals. Anti-β-actin antibody, 3-methyladenine, 2-deoxy-D-glucose (2-DG), and sodium azide (NaN_3) were obtained from Sigma Aldrich. Anti-FVIII antibody (GMA012) was obtained from Green Mountain. [^{35}S]-Methionine/Cysteine was obtained from MP Biologicals. Mouse and rabbit horseradish peroxidase conjugated secondary antibodies, Prolong Antifade Gold and Complete Protease Inhibitor Cocktail were obtained from Promega. Supersignal West Pico ECL was obtained from Thermo. Mouse FAB fragments, Dylight 549 conjugated anti-mouse fab fragments and Texas-Red conjugated anti-mouse secondary were obtained from Jackson Immunoresearch.

Mice

Male *C57BL/6J* mice were purchased from Jackson Laboratory and maintained at the Sanford-Burnham-Prebys Medical Discovery Institute animal facility. Mice were euthanized by CO_2 inhalation for liver harvest. All animal protocols were reviewed and approved by the Institutional Animal Care and Use Committee at the SBP Medical Discovery Institute.

Hydrodynamic tail vein injection of plasmid DNA and HCC development

The expression vectors for BDD and N6 were previously described (18). Six wk-old male mice were used for these experiments. Hydrodynamic tail vein DNA injection was performed according to previous publications (17, 42). In summary, 100μg plasmid DNA was diluted in 2.5ml saline and injected into mice through the tail vein. One wk after the injection, mice were fed 60% HFD for 65 wks after which their livers were harvested for tumor evaluation.

Glucose depletion and repletion

For glucose depletion, cells were treated with ATP-depleting medium (glucose-free DMEM containing 20 mM 2-DG and 10 mM NaN_3) for 2 hr. To replete glucose, fresh media was replaced for the indicated time. Cycloheximide (CHX) at a final concentration of 10 μg/mL was added to

the repletion media where indicated.

Factor VIII activity and antigen analysis

FVIII activity was measured by a 1-stage activated thromboplastin time (aPTT) clotting assay on an MLA Electra 750 fibrinometer (Medical Laboratory Automation, Pleasantville, NY) by reconstitution of human FVIII-deficient plasma. The FVIII plasma standard was FACT plasma (normal pooled plasma) from George King Biomedical. FVIII antigen was quantified by an anti-FVIII sandwich enzyme-linked immunosorbent assay (ELISA) method using the Affinity Biologicals FVIII:C-EIA commercial kit according to the manufacturers' instructions.

Metabolic labeling

Cells were subcultured 24 hr prior to labeling in 60 mm dishes (approximately 10^6 cells/plate) and were 80% confluent at the time of labeling. Cells were washed twice in cys/met free DMEM and incubated in cys/met-free DMEM for 10 min prior to labeling. Cells were labeled in 0.5 ml Cys/Met free DMEM containing 100 μCi/mL (BDD-FVIII and N6-FVIII) for 20 min and chased for the indicated times with conditioned medium (either 2-DG and NaN_3-containing medium or normal medium) containing excess unlabeled Cys and Met and 10 μg/ml aprotinin. For glucose-depletion/repletion conditions, depleting medium was removed after 2 hr and replaced with normal medium containing excess unlabeled Cys and Met and aprotinin as above. At the end of the chase period, conditioned media was collected. Cells were rinsed three times in phosphate buffered saline (PBS) and harvested in 1 ml lysis buffer [50 mM Tris-HCl, pH 7.4, 150 mM NaCl, 0.1% (v/v) Triton X-100, and 1% (v/v) IGEPAL] containing Complete Protease Inhibitor Cocktail and 1 mM phenylmethylsulfonyl fluoride. Lysates were incubated on ice 30 min, followed by centrifugation at 15,000 x g for 10 min. Post-nuclear supernatant was then assayed for protein content using BCA assay (Bio-Rad). Equal amounts of protein and corresponding amounts of media were subjected to FVIII immunoprecipitation (IP) using anti-FVIII coupled Sepharose CL-4B beads at 4˚C overnight. IPs were washed 4 times with lysis buffer and proteins were separated by reducing SDS-PAGE. IP'd proteins were visualized by autoradiography and band intensities were quantified using ImageQuant normal media for indicated times. CHX at a final concentration of 10 μg/mL was added to the repletion media where indicated.

Interaction of BDD and N6 with BiP *in vivo.*

The *BiP-Flag* mice were generated as described (46). Mice were fed a regular mouse chow diet. Induction of BiP-Flag expression was initiated at the age of 6 wks by transduction with AAV8-TGB-Cre (46). AAV8-TGB-Cre-transdcued wild type littermates were used as controls. At 6 wks

after AAV8-TGB-Cre-transduction, the mice received pMT2 empty vector, BDD vector, or N6 vector through hydrodynamic tail vein DNA injection (17) and were sacrificed to collect liver tissues 46 hr post-vector DNA injection.

Liver samples were harvested in lysis buffer [0.15 mM NaCl, 0.5% Triton X-100, 20 mM HEPES, pH 7.4, 1x Protease inhibitor cocktail (Fisher)]. The liver lysates were centrifuged at 10K x g for 10 min and the resultant supernatants were used for anti-Flag or anti-FVIII IP. For anti-Flag IP, 150 μg of lysate proteins in 400 μl of lysis buffer was mixed with 15 μl of M2 anti-Flag magnetic beads (Sigma) and incubated with rotation at 4°C for 4 hr. At the end of this incubation, the anti-Flag beads were washed 3 x with ice-cold lysis buffer (1 ml each). Direct anti-FVIII IP was performed in a similar manner except that 75 μg of lysate protein and 25 μl of anti-FVIII-coupled agarose beads (26) were used in place of anti-Flag beads. Proteins in the washed anti-Flag and anti-FVIII beads were eluted with SDS-PAGE loading buffer, separated by SDS-PAGE under reducing conditions and transferred onto Nitrocellulose membranes for Western blotting. A mouse anti-human FVIII antibody (GAM012, Green Mountain) was used for BDD and N6 detection.

***Ex vivo* experiment with mouse-passaged primary human hepatocytes**

Mouse-passed primary human hepatocytes (PHH) were prepared and cultured as described (47). They were transduced with a lentiviral vector expressing a codon-optimized form of SQ-BDD coding sequence (Lenti-BDD) (12) at the indicated doses 3 days after isolation and being cultured *ex vivo* and harvested for Western blot analysis 10 days after transduction.

Antibodies used were as follows: Rabbit anti-BiP, rabbit anti-phospho eIF2α and rabbit anti-eIF2α were from Cell Signaling Technology, (Danvers, MA). Mouse anti-human FVIII was from Green Mountain Antibodies (Burlington, VT); Mouse anti-CHOP was from Santa Cruz Biotechnology (Santa Cruz, CA); Rabbit anti-CRELD2 and mouse anti-hepcidin antibodies were from Proteintech (Rosemont, IL) and Novus Biologicals (Burlington, Vt), respectively. Mouse anti-beta actin was from ThermoFisher (Waltham, MA).

Histology and Immunohistochemistry staining

Formalin-fixed paraffin-embedded (FFPE) blocks of mouse livers were prepared from empty vector, BDD, and N6-transduced mice. Tissue fixation and paraffin embedding was performed following routine methods. Four μm-thick serial sections were cut from each FFPE block and adhered to charged glass slides (Superfrost Plus; Fisher Scientific, Waltham, MA, USA). Sections were incubated at 60°C for 1 hr prior to deparaffinization in xylene and then rehydrated in 100%, 95%, and double-distilled water successively. Sections were heat-induced in retrieval buffer at pH

6.0, incubated with peroxidase block (Dako, Mississauga, ON, Canada) for 20 min followed by blocking (5% goat serum in 1% PBS-T) for 1 hr. Sections were then incubated overnight at 4°C with primary antibodies diluted in blocking buffer. Primary antibodies used for this study were: rabbit anti-GS (Glutamine Synthetase: Abcam, Cambridge, UK, ab176562; dilution 1:1000), rabbit anti-CD34 (Abcam, Cambridge, UK, ab81289; dilution 1:2500), rabbit anti-CTNNB1 (β-catenin: Abcam, Cambridge, UK, ab223075; dilution 1:4800), rabbit anti-CD44 (Abcam, Cambridge, UK, ab157107; dilution 1:2500), rabbit anti-GPC3 (Glypican-3: LSBio, Seattle, USA, LS-B13373; dilution 1:4000), rabbit anti-BiP (Binding Immunoglobulin Protein: Cell Signaling Technology, Massachusetts, USA, #3177; dilution 1:600). The detection system used was the EnVision+ System-HRP kit (Dako, K4007). Sections were counterstained with hematoxylin prior to dehydration and mounted with Permount (Fisher, SP-15-100). The first section of each series was stained with Hematoxylin and Eosin (H&E) and the fifth section was stained with reticulin (Abcam, #ab150684) for an initial histopathological assessment. Immunohistochemistry with Thio-S and FVIII antibodies was performed as previously described **(26)**.

Scoring analysis

Slides were scanned using the Aperio AT Turbo system at 20x magnification and viewed using the Aperio Image Scope system. The positivity [Total number of positive pixels divided by total number of pixels: (NTotal – Nn)/(NTotal)] was assessed using the positive pixel count algorithm from the ImageScope software (positive pixel count V9, Aperio, Inc.). The algorithm outputs a strong, moderate, and weak intensity range. The total signal positivity was used to quantify all immunohistochemistry markers where only the strong signal positivity was used as a measure of total positivity of apoptotic cells for TUNEL assay positivity quantification. Signal positivity was analyzed at the central tumor, the interface and distal normal liver.

Histopathological analysis

All slides were analyzed, in a blinded fashion, by a board-certified pathologist who evaluated the presence of hepatocellular adenomas and carcinomas. The following are the stains used to confirm the lesions and to evaluate whether they represent adenomas (benign disease) or carcinomas. Reticulin staining is intended to demonstrate reticular fibers surrounding tumor cells. Tumors that retain a reticulin network are generally benign or pre-neoplastic, whereas HCC loses the reticulin fiber normal architecture (71). CD34 is a marker of “capillarization”, a process by which sinusoid endothelial cells lose their fenestration. CD34 demonstrates neovascularization in HCC, while nontumorous hepatic sinusoids do not stain with CD34 (72). However, it was previously reported that in some cases, CD34 may occur diffusely or in areas of hepatocellular

adenoma (Brunt et al., 2012). Glutamine synthetase (GS) stains positively for zone 3 of the liver parenchyma. HCCs show strong positive staining while adenomas show negative staining. Similarly, glypican 3 (GPC3) was identified as a tumor marker for the diagnosis of HCC due to its specificity and sensitivity (54). GPC3 stains negatively HCC. β-catenin shows membranous positive staining on normal hepatocytes. Activation of β-catenin due to a missense mutation leads cytoplasmic and nuclear accumulation of β-catenin which is suggestive of malignant transformation (73). Finally, CD44 is an adhesion molecule widely found on lymphoid and Kupffer cell types in normal liver (74). During malignant transformation, CD44 is upregulated in HCC progenitor cells and is a marker for tumor-initiating stem-like cells (75). HCC lesions that show a membranous staining pattern are indicative of neoplastic stem cell proliferation (76).

Statistical Analyses

Statistical analyses were performed using GraphPad Prism 9. Chi-square test was used for comparing of tumor incidence between BDD and N6 groups. A p value < 0.05 was regarded as statistically significant. Statistical analysis for immunohistochemistry was performed with a two-tailed Student's *t*-test. *P* values of <0.05 were considered significant ($p < 0.05$ *, $p < 0.01$ **, $p < 0.001$ ***).

Acknowledgments

This work was supported by NIH grants CA198103 and DK113171 and HL160472 to R.J.K. and in part by the NIDDK-funded San Diego Digestive Diseases Research Center (P30DK 120515).

Author Contributions:

R.J.K. conceived the project, designed and interpreted experiments, and wrote the manuscript with Z.C. and A. K.. A.K., Z.C., R.D., C.L., L.G., J.M., J.Y. and C.Z. performed various *in vivo* and *in vitro* experiments. Z.G., A.L. and P.M. provided expert consultation and supervision on tumor analyses. Y.D.J. and R.W.H. interpreted data and edited the manuscript. R.J.K. supported the study.

Figure Legends

Figure 1. Hepatocyte responses to wtFVIII, BDD, and N6 upon hydrodynamic tail vein injection of vector DNA into mice. Relative FVIII secretion efficiency, activation of the UPR, production of reactive oxygen species (ROS), induction of apoptosis, and the ability for BHA to improve secretion (17). a1-3=acidic regions. N-glycosylation sites (N-gly) and disulfide bonds (s-s) are depicted. Red bracket indicates residues from the B domain of wtFVIII that were retained in N6.

Figure 2. Reversible aggregation of BDD and N6 expressed in CHO cells. A) FVIII aggregates induced by glucose depletion begin to resolve at 1 hr following glucose repletion. CHO cells that express BDD or N6 were treated with either normal media or glucose-free media containing 10 mM 2DG and 20 mM azide (2DG+NaN_3). After 2 hr, cells were harvested or allowed to recover in complete media for the indicated times, or complete media with 10 μg/ml CHX. Cell lysates were filtered through nitrocellulose (left) or cellulose acetate (right) membranes and probed with FVIII or β-actin antibodies. Analysis of β-actin is from BDD expressing CHO cells. **B) Reversible retention and secretion of active FVIII in CHO cells.** [^{35}S]-Met/Cys pulse-chase and aPTT analysis of BDD and N6 expressed in CHO cells. CHO cells were treated in parallel as in Panel A. CHO cells were pulse-labeled for 20 min and then chased for 20 min with media containing excess unlabeled Met/Cys to complete synthesis of nascent chains (lane 1) before being treated with either normal media (lanes 2-3) or glucose-free media containing 10 mM 2DG and 20 mM NaN_3. After 2 hr cells were harvested (lane 4) or allowed to recover in complete media for increasing times (lanes 5-8), or complete media with CHX (lane 9). Lysates and media were collected at indicated time points for FVIII IP and reducing SDS-PAGE. For FVIII aPPT activity assay of media, cells were treated in parallel, but not pulse-labeled. Lanes: 1: Untreated, 20' chase; 2: Untreated 120' chase; 3: Untreated 240' chase; 4-9: 2DG for 120'; 5: 2-DG + 30' recovery; 6: 2-DG + 60' recovery; 7: 2DG + 120' recovery; 8: 2DG + 240' recovery; 9: 2DG + 240' recovery + CHX.

Figure 3: BDD expression in hepatocytes *in vivo* causes accumulation of amyloid-like aggregates that colocalize with FVIII in liver sections. Liver sections were prepared from mice injected with the indicated vector DNAs as described (17) and stained for FVIII (red) and Thio-S (green) (26).

Figure 4. Epitope-tagging of the endogenous murine BIP/GRP78/*Hspa5* locus demonstrates misfolding of BDD *in vivo*. A) A diagram illustrating location of insertion of 3x Flag tag to C-terminal region of BiP; **B)** Western blot demonstrating similar changes in hepatic levels of endogenous wtBiP (BiP) and BiP-Flag in mice heterozygous for *BiP-Flag* allele (10 days after activation of BiP-Flag expression in the liver) in response to treatment with tunicamycin for 24 hr. C. Co-IP of BDD (lanes 13 &14) and N6 (lanes 17 & 18) from liver lysates of BDD or N6 vector-injected *BiP-Flag* homozygous mice (*BiP-Flag*$^{+/+}$) with anti-Flag magnetic beads. Direct FVIII IP using anti-FVIII agarose beads demonstrates the relative levels of BDD and N6 in the liver samples (lanes 21-24).

Figure 5. BDD expression induces the UPR in primary human hepatocytes (PHH). PHH were transduced with a lentiviral vector expressing a codon-optimized form of SQ-BDD (Lenti-BDD) at the indicated vector doses and cultured in a hepatocyte-defined medium. The transduced PHH were harvested for western blot analysis 10 days post-transduction. Each lane represents individual culture well. The numerical numbers represent averaged fold changes after correction with loading control β-actin.

Figure 6. Transient FVIII expression in hepatocytes causes liver tumors in mice in the context of high-fat diet (HFD) feeding. WT *C57BL/6J* male mice were injected with pMT empty vector, N6 or BDD DNA vectors by hydrodynamic tail vein injection. **A)** Plasma FVIII levels at 24 hr after vector DNA injection. Data shown are Mean ± SE (N=4 for pMT-empty vector and BDD, N=5 for N6). **B)** Incidence of liver tumors in BDD- or N6-vector injected mice after a 65-wk-HFD treatment. The difference between the two groups (N6 & BDD) were tested for statistical significance using the Chi-square test (degrees of freedom=1, 95% confidence intervals). **C)** HCC but not adenoma exhibited positivity for glutamine synthase (GS) staining.

Figure 7. HCC in BDD mice have higher BiP levels than HCC in N6 mice. Total Positivity levels (%) of BiP quantification of N6 and BDD mouse cohorts. Central tumor, interface normal, and distal normal regions of interest were quantified using the total positive pixel per count algorithm from Aperio software represented as positivity percentage (pixels/Area). **A)** Comparison of positivity (%) levels of adenoma and HCC tumor types for N6 and BDD cohorts. Statistical analyses were performed using a two-tailed Student's *t*-test where *p*-values of <0.05 were considered to be significant ($p < 0.05$ *, $p < 0.01$ **, $p < 0.001$ ***). **B & C)** Representation of BiP immunohistochemistry. N6 and BDD cohort samples (N6-5, N6-9, BDD-1, and BDD-3) for HCC (**B**) and Adenomas (**C**).

Figure S1. Liver surface tumors in mice injected with N6 vector DNA. Mice were injected with BDD, N6, or empty vector DNA and treated with a high-fat diet as described in Methods and legend to Fig. 6. **A)** Distribution of HCC and adenomas among liver tumors in the N6 cohort. **B)** Positivity for glutamine synthase (GS) stains was observed in HCC but not in adenoma of the N6 mice.

Figure S2. Representative immunohistochemistry characterization of HCC samples (BDD8 & N6-2). Serial sections were stained for H&E: Hematoxylin and Eosin, reticulin, CD34, glutamine synthetase, glypican-3, β-catenin, and CD44.

Figure S3. Summary of immunohistochemistry of BiP in tumors of BDD and N6 cohorts.

Table S1. Immunohistochemistry characterization of the BDD cohort samples.

Table S2. Immunohistochemistry characterization of the N6 cohort samples.

References

1. Seaman CD, Xavier F, Ragni MV. Hemophilia A (Factor VIII Deficiency). Hematol Oncol Clin North Am. 2021;35(6):1117-29. Epub 2021/08/15. doi: 10.1016/j.hoc.2021.07.006. PubMed PMID: 34389199.
2. Meeks SL, Batsuli G. Hemophilia and inhibitors: current treatment options and potential new therapeutic approaches. Hematology Am Soc Hematol Educ Program. 2016;2016(1):657-62. Epub 2016/12/04. doi: 10.1182/asheducation-2016.1.657. PubMed PMID: 27913543; PMCID: PMC6142469.
3. Jiang R, Monroe T, McRogers R, Larson PJ. Manufacturing challenges in the commercial production of recombinant coagulation factor VIII. Haemophilia. 2002;8 Suppl 2:1-5. Epub 2002/04/23. doi: 10.1046/j.1351-8216.2001.00115.x. PubMed PMID: 11966844.
4. Pipe SW. The promise and challenges of bioengineered recombinant clotting factors. J Thromb Haemost. 2005;3(8):1692-701. Epub 2005/08/17. doi: 10.1111/j.1538-7836.2005.01367.x. PubMed PMID: 16102035.
5. Pittman DD, Kaufman RJ. Structure-function relationships of factor VIII elucidated through recombinant DNA technology. Thromb Haemost. 1989;61(2):161-5. Epub 1989/04/25. PubMed PMID: 2501893.
6. Everett LA, Cleuren AC, Khoriaty RN, Ginsburg D. Murine coagulation factor VIII is synthesized in endothelial cells. Blood. 2014;123(24):3697-705. Epub 2014/04/11. doi: 10.1182/blood-2014-02-554501. PubMed PMID: 24719406; PMCID: PMC4055920.
7. Toole JJ, Pittman DD, Orr EC, Murtha P, Wasley LC, Kaufman RJ. A large region (approximately equal to 95 kDa) of human factor VIII is dispensable for in vitro procoagulant activity. Proc Natl Acad Sci U S A. 1986;83(16):5939-42. Epub 1986/08/01. doi: 10.1073/pnas.83.16.5939. PubMed PMID: 3016730; PMCID: PMC386412.
8. Pittman DD, Alderman EM, Tomkinson KN, Wang JH, Giles AR, Kaufman RJ. Biochemical, immunological, and in vivo functional characterization of B-domain-deleted factor VIII. Blood. 1993;81(11):2925-35. Epub 1993/06/01. PubMed PMID: 8499631.
9. Lusher JM, Lee CA, Kessler CM, Bedrosian CL, ReFacto Phase 3 Study G. The safety and efficacy of B-domain deleted recombinant factor VIII concentrate in patients with severe haemophilia A. Haemophilia. 2003;9(1):38-49. Epub 2003/02/01. doi: 10.1046/j.1365-2516.2003.00708.x. PubMed PMID: 12558777.
10. Lusher JM, Roth DA. The safety and efficacy of B-domain deleted recombinant factor VIII concentrates in patients with severe haemophilia A: an update. Haemophilia. 2005;11(3):292-3. Epub 2005/05/07. doi: 10.1111/j.1365-2516.2005.01099.x. PubMed PMID: 15876278.
11. Di Paola J, Smith MP, Klamroth R, Mannucci PM, Kollmer C, Feingold J, Kessler C, Pollmann H, Morfini M, Udata C, Rothschild C, Hermans C, Janco R. ReFacto and Advate: a single-dose, randomized, two-period crossover pharmacokinetics study in subjects with haemophilia A. Haemophilia. 2007;13(2):124-30. Epub 2007/02/09. doi: 10.1111/j.1365-2516.2006.01420.x. PubMed PMID: 17286764.
12. Ward NJ, Buckley SM, Waddington SN, Vandendriessche T, Chuah MK, Nathwani AC, McIntosh J, Tuddenham EG, Kinnon C, Thrasher AJ, McVey JH. Codon optimization of human factor VIII cDNAs leads to high-level expression. Blood. 2011;117(3):798-807. Epub 2010/11/03. doi: 10.1182/blood-2010-05-282707. PubMed PMID: 21041718.
13. Rangarajan S, Walsh L, Lester W, Perry D, Madan B, Laffan M, Yu H, Vettermann C, Pierce GF, Wong WY, Pasi KJ. AAV5-Factor VIII Gene Transfer in Severe Hemophilia A. N Engl J Med. 2017;377(26):2519-30. Epub 2017/12/12. doi: 10.1056/NEJMoa1708483. PubMed

PMID: 29224506.
14. Pasi KJ, Rangarajan S, Mitchell N, Lester W, Symington E, Madan B, Laffan M, Russell CB, Li M, Pierce GF, Wong WY. Multiyear Follow-up of AAV5-hFVIII-SQ Gene Therapy for Hemophilia A. N Engl J Med. 2020;382(1):29-40. Epub 2020/01/02. doi: 10.1056/NEJMoa1908490. PubMed PMID: 31893514.
15. Grimm D, Kay MA. From virus evolution to vector revolution: use of naturally occurring serotypes of adeno-associated virus (AAV) as novel vectors for human gene therapy. Curr Gene Ther. 2003;3(4):281-304. Epub 2003/07/23. doi: 10.2174/1566523034578285. PubMed PMID: 12871018.
16. Arruda VR, Doshi BS. Gene Therapy for Hemophilia: Facts and Quandaries in the 21st Century. Mediterr J Hematol Infect Dis. 2020;12(1):e2020069. Epub 2020/09/22. doi: 10.4084/MJHID.2020.069. PubMed PMID: 32952980; PMCID: PMC7485465.
17. Malhotra JD, Miao H, Zhang K, Wolfson A, Pennathur S, Pipe SW, Kaufman RJ. Antioxidants reduce endoplasmic reticulum stress and improve protein secretion. Proc Natl Acad Sci U S A. 2008;105(47):18525-30. Epub 2008/11/18. doi: 10.1073/pnas.0809677105. PubMed PMID: 19011102; PMCID: PMC2587584.
18. Miao HZ, Sirachainan N, Palmer L, Kucab P, Cunningham MA, Kaufman RJ, Pipe SW. Bioengineering of coagulation factor VIII for improved secretion. Blood. 2004;103(9):3412-9. Epub 2004/01/17. doi: 10.1182/blood-2003-10-3591. PubMed PMID: 14726380.
19. Nichols WC, Seligsohn U, Zivelin A, Terry VH, Hertel CE, Wheatley MA, Moussalli MJ, Hauri HP, Ciavarella N, Kaufman RJ, Ginsburg D. Mutations in the ER-Golgi intermediate compartment protein ERGIC-53 cause combined deficiency of coagulation factors V and VIII. Cell. 1998;93(1):61-70. Epub 1998/04/18. doi: 10.1016/s0092-8674(00)81146-0. PubMed PMID: 9546392.
20. Pipe SW, Morris JA, Shah J, Kaufman RJ. Differential interaction of coagulation factor VIII and factor V with protein chaperones calnexin and calreticulin. J Biol Chem. 1998;273(14):8537-44. Epub 1998/05/09. doi: 10.1074/jbc.273.14.8537. PubMed PMID: 9525969.
21. Moussalli M, Pipe SW, Hauri HP, Nichols WC, Ginsburg D, Kaufman RJ. Mannose-dependent endoplasmic reticulum (ER)-Golgi intermediate compartment-53-mediated ER to Golgi trafficking of coagulation factors V and VIII. J Biol Chem. 1999;274(46):32539-42. Epub 1999/11/07. doi: 10.1074/jbc.274.46.32539. PubMed PMID: 10551804.
22. Cunningham MA, Pipe SW, Zhang B, Hauri HP, Ginsburg D, Kaufman RJ. LMAN1 is a molecular chaperone for the secretion of coagulation factor VIII. J Thromb Haemost. 2003;1(11):2360-7. Epub 2003/11/25. doi: 10.1046/j.1538-7836.2003.00415.x. PubMed PMID: 14629470.
23. Zhang B, Cunningham MA, Nichols WC, Bernat JA, Seligsohn U, Pipe SW, McVey JH, Schulte-Overberg U, de Bosch NB, Ruiz-Saez A, White GC, Tuddenham EG, Kaufman RJ, Ginsburg D. Bleeding due to disruption of a cargo-specific ER-to-Golgi transport complex. Nat Genet. 2003;34(2):220-5. Epub 2003/04/30. doi: 10.1038/ng1153. PubMed PMID: 12717434.
24. Zhang B, McGee B, Yamaoka JS, Guglielmone H, Downes KA, Minoldo S, Jarchum G, Peyvandi F, de Bosch NB, Ruiz-Saez A, Chatelain B, Olpinski M, Bockenstedt P, Sperl W, Kaufman RJ, Nichols WC, Tuddenham EG, Ginsburg D. Combined deficiency of factor V and factor VIII is due to mutations in either LMAN1 or MCFD2. Blood. 2006;107(5):1903-7. Epub 2005/11/24. doi: 10.1182/blood-2005-09-3620. PubMed PMID: 16304051; PMCID: PMC1895703.
25. Tagliavacca L, Wang Q, Kaufman RJ. ATP-dependent dissociation of non-disulfide-linked aggregates of coagulation factor VIII is a rate-limiting step for secretion. Biochemistry. 2000;39(8):1973-81. Epub 2000/02/24. doi: 10.1021/bi991896r. PubMed PMID: 10684647.
26. Poothong J, Pottekat A, Siirin M, Campos AR, Paton AW, Paton JC, Lagunas-Acosta J, Chen Z, Swift M, Volkmann N, Hanein D, Yong J, Kaufman RJ. Factor VIII exhibits chaperone-

dependent and glucose-regulated reversible amyloid formation in the endoplasmic reticulum. Blood. 2020;135(21):1899-911. Epub 2020/03/05. doi: 10.1182/blood.2019002867. PubMed PMID: 32128578; PMCID: PMC7243144.
27. Sabatino DE. Clogging up the pipeline: factor VIII aggregates. Blood. 2020;135(21):1825-7. Epub 2020/05/22. doi: 10.1182/blood.2020005450. PubMed PMID: 32437559.
28. Pasi KJ, Laffan M, Rangarajan S, Robinson TM, Mitchell N, Lester W, Symington E, Madan B, Yang X, Kim B, Pierce GF, Wong WY. Persistence of haemostatic response following gene therapy with valoctocogene roxaparvovec in severe haemophilia A. Haemophilia. 2021. Epub 2021/08/12. doi: 10.1111/hae.14391. PubMed PMID: 34378280.
29. Pierce GF. Gene Therapy for Hemophilia: Are Expectations Matching Reality? Mol Ther. 2020;28(10):2097-8. Epub 2020/09/24. doi: 10.1016/j.ymthe.2020.09.019. PubMed PMID: 32966774; PMCID: PMC7544995.
30. Pierce GF, Kaczmarek R, Noone D, O'Mahony B, Page D, Skinner MW. Gene therapy to cure haemophilia: Is robust scientific inquiry the missing factor? Haemophilia. 2020;26(6):931-3. Epub 2020/09/11. doi: 10.1111/hae.14131. PubMed PMID: 32909632.
31. Sheridan C. A reprieve from hemophilia A, but for how long? Nat Biotechnol. 2020;38(10):1107-9. Epub 2020/10/07. doi: 10.1038/s41587-020-0693-y. PubMed PMID: 33020631.
32. Batty P, Lillicrap D. Hemophilia Gene Therapy: Approaching the First Licensed Product. Hemasphere. 2021;5(3):e540. Epub 2021/02/20. doi: 10.1097/HS9.0000000000000540. PubMed PMID: 33604517; PMCID: PMC7886458 PB has received research support from BioMarin, Grifols, and Octapharma.
33. Sung H, Ferlay J, Siegel RL, Laversanne M, Soerjomataram I, Jemal A, Bray F. Global Cancer Statistics 2020: GLOBOCAN Estimates of Incidence and Mortality Worldwide for 36 Cancers in 185 Countries. CA Cancer J Clin. 2021;71(3):209-49. Epub 2021/02/05. doi: 10.3322/caac.21660. PubMed PMID: 33538338.
34. White DL, Thrift AP, Kanwal F, Davila J, El-Serag HB. Incidence of Hepatocellular Carcinoma in All 50 United States, From 2000 Through 2012. Gastroenterology. 2017;152(4):812-20 e5. Epub 2016/11/28. doi: 10.1053/j.gastro.2016.11.020. PubMed PMID: 27889576; PMCID: PMC5346030.
35. Ahmed O, Liu L, Gayed A, Baadh A, Patel M, Tasse J, Turba U, Arslan B. The Changing Face of Hepatocellular Carcinoma: Forecasting Prevalence of Nonalcoholic Steatohepatitis and Hepatitis C Cirrhosis. J Clin Exp Hepatol. 2019;9(1):50-5. Epub 2019/02/16. doi: 10.1016/j.jceh.2018.02.006. PubMed PMID: 30765939; PMCID: PMC6363953.
36. Wang M, Kaufman RJ. The impact of the endoplasmic reticulum protein-folding environment on cancer development. Nat Rev Cancer. 2014;14(9):581-97. Epub 2014/08/26. doi: 10.1038/nrc3800. PubMed PMID: 25145482.
37. Wang M, Kaufman RJ. Protein misfolding in the endoplasmic reticulum as a conduit to human disease. Nature. 2016;529(7586):326-35. Epub 2016/01/23. doi: 10.1038/nature17041. PubMed PMID: 26791723.
38. Malhi H, Kaufman RJ. Endoplasmic reticulum stress in liver disease. J Hepatol. 2011;54(4):795-809. Epub 2010/12/15. doi: 10.1016/j.jhep.2010.11.005. PubMed PMID: 21145844; PMCID: PMC3375108.
39. Lebeaupin C, Vallee D, Hazari Y, Hetz C, Chevet E, Bailly-Maitre B. Endoplasmic reticulum stress signalling and the pathogenesis of non-alcoholic fatty liver disease. J Hepatol. 2018;69(4):927-47. Epub 2018/06/26. doi: 10.1016/j.jhep.2018.06.008. PubMed PMID: 29940269.
40. Rutkowski DT. Liver function and dysfunction - a unique window into the physiological reach of ER stress and the unfolded protein response. FEBS J. 2019;286(2):356-78. Epub 2018/01/24. doi: 10.1111/febs.14389. PubMed PMID: 29360258; PMCID: PMC6056347.

41. Nakagawa H, Umemura A, Taniguchi K, Font-Burgada J, Dhar D, Ogata H, Zhong Z, Valasek MA, Seki E, Hidalgo J, Koike K, Kaufman RJ, Karin M. ER stress cooperates with hypernutrition to trigger TNF-dependent spontaneous HCC development. Cancer Cell. 2014;26(3):331-43. Epub 2014/08/19. doi: 10.1016/j.ccr.2014.07.001. PubMed PMID: 25132496; PMCID: PMC4165611.
42. Liu F, Song Y, Liu D. Hydrodynamics-based transfection in animals by systemic administration of plasmid DNA. Gene Ther. 1999;6(7):1258-66. Epub 1999/08/24. doi: 10.1038/sj.gt.3300947. PubMed PMID: 10455434.
43. Pobre KFR, Poet GJ, Hendershot LM. The endoplasmic reticulum (ER) chaperone BiP is a master regulator of ER functions: Getting by with a little help from ERdj friends. J Biol Chem. 2019;294(6):2098-108. Epub 2018/12/20. doi: 10.1074/jbc.REV118.002804. PubMed PMID: 30563838; PMCID: PMC6369273.
44. Ng DT, Watowich SS, Lamb RA. Analysis in vivo of GRP78-BiP/substrate interactions and their role in induction of the GRP78-BiP gene. Mol Biol Cell. 1992;3(2):143-55. Epub 1992/02/01. doi: 10.1091/mbc.3.2.143. PubMed PMID: 1550958; PMCID: PMC275514.
45. Preissler S, Chambers JE, Crespillo-Casado A, Avezov E, Miranda E, Perez J, Hendershot LM, Harding HP, Ron D. Physiological modulation of BiP activity by trans-protomer engagement of the interdomain linker. Elife. 2015;4:e08961. Epub 2015/10/17. doi: 10.7554/eLife.08961. PubMed PMID: 26473973; PMCID: PMC4608358.
46. Peng Y, Chen Z, Peter A, Kaufman RJ. Epitope-tagging of the endogenous murine BiP/GRP78/Hspa5 locus allows direct analysis of the BiP interactome and protein misfolding in vivo. bioRxiv. 2020:2020.01.01.892539. doi: 10.1101/2020.01.01.892539.
47. Michailidis E, Vercauteren K, Mancio-Silva L, Andrus L, Jahan C, Ricardo-Lax I, Zou C, Kabbani M, Park P, Quirk C, Pyrgaki C, Razooky B, Verhoye L, Zoluthkin I, Lu WY, Forbes SJ, Chiriboga L, Theise ND, Herzog RW, Suemizu H, Schneider WM, Shlomai A, Meuleman P, Bhatia SN, Rice CM, de Jong YP. Expansion, in vivo-ex vivo cycling, and genetic manipulation of primary human hepatocytes. Proc Natl Acad Sci U S A. 2020;117(3):1678-88. Epub 2020/01/10. doi: 10.1073/pnas.1919035117. PubMed PMID: 31915293; PMCID: PMC6983380.
48. Vecchi C, Montosi G, Zhang K, Lamberti I, Duncan SA, Kaufman RJ, Pietrangelo A. ER stress controls iron metabolism through induction of hepcidin. Science. 2009;325(5942):877-80. Epub 2009/08/15. doi: 10.1126/science.1176639. PubMed PMID: 19679815; PMCID: PMC2923557.
49. Oh-hashi K, Koga H, Ikeda S, Shimada K, Hirata Y, Kiuchi K. CRELD2 is a novel endoplasmic reticulum stress-inducible gene. Biochem Biophys Res Commun. 2009;387(3):504-10. Epub 2009/07/21. doi: 10.1016/j.bbrc.2009.07.047. PubMed PMID: 19615339.
50. Boyle ST, Poltavets V, Kular J, Pyne NT, Sandow JJ, Lewis AC, Murphy KJ, Kolesnikoff N, Moretti PAB, Tea MN, Tergaonkar V, Timpson P, Pitson SM, Webb AI, Whitfield RJ, Lopez AF, Kochetkova M, Samuel MS. Publisher Correction: ROCK-mediated selective activation of PERK signalling causes fibroblast reprogramming and tumour progression through a CRELD2-dependent mechanism. Nat Cell Biol. 2020;22(7):908. Epub 2020/06/06. doi: 10.1038/s41556-020-0539-3. PubMed PMID: 32499616.
51. Liu GM, Zeng HD, Zhang CY, Xu JW. Key genes associated with diabetes mellitus and hepatocellular carcinoma. Pathol Res Pract. 2019;215(11):152510. Epub 2019/10/09. doi: 10.1016/j.prp.2019.152510. PubMed PMID: 31591054.
52. Kern P, Balzer NR, Blank N, Cygon C, Wunderling K, Bender F, Frolov A, Sowa JP, Bonaguro L, Ulas T, Homrich M, Kiermaier E, Thiele C, Schultze JL, Canbay A, Bauer R, Mass E. Creld2 function during unfolded protein response is essential for liver metabolism homeostasis. FASEB J. 2021;35(10):e21939. Epub 2021/09/23. doi: 10.1096/fj.202002713RR. PubMed PMID: 34549824.
53. Cui S, Hano H, Sakata A, Harada T, Liu T, Takai S, Ushigome S. Enhanced CD34

expression of sinusoid-like vascular endothelial cells in hepatocellular carcinoma. Pathol Int. 1996;46(10):751-6. Epub 1996/10/01. doi: 10.1111/j.1440-1827.1996.tb03544.x. PubMed PMID: 8916144.
54. Wasfy RE, Shams Eldeen AA. Roles of Combined Glypican-3 and Glutamine Synthetase in Differential Diagnosis of Hepatocellular Lesions. Asian Pac J Cancer Prev. 2015;16(11):4769-75. Epub 2015/06/25. doi: 10.7314/apjcp.2015.16.11.4769. PubMed PMID: 26107238.
55. Di Tommaso L, Franchi G, Park YN, Fiamengo B, Destro A, Morenghi E, Montorsi M, Torzilli G, Tommasini M, Terracciano L, Tornillo L, Vecchione R, Roncalli M. Diagnostic value of HSP70, glypican 3, and glutamine synthetase in hepatocellular nodules in cirrhosis. Hepatology. 2007;45(3):725-34. Epub 2007/02/28. doi: 10.1002/hep.21531. PubMed PMID: 17326147.
56. Pfaffenbach KT, Lee AS. The critical role of GRP78 in physiologic and pathologic stress. Curr Opin Cell Biol. 2011;23(2):150-6. Epub 2010/10/26. doi: 10.1016/j.ceb.2010.09.007. PubMed PMID: 20970977; PMCID: PMC3043145.
57. Luo C, Xiong H, Chen L, Liu X, Zou S, Guan J, Wang K. GRP78 Promotes Hepatocellular Carcinoma proliferation by increasing FAT10 expression through the NF-kappaB pathway. Exp Cell Res. 2018;365(1):1-11. Epub 2018/02/20. doi: 10.1016/j.yexcr.2018.02.007. PubMed PMID: 29458176.
58. Chen WT, Zhu G, Pfaffenbach K, Kanel G, Stiles B, Lee AS. GRP78 as a regulator of liver steatosis and cancer progression mediated by loss of the tumor suppressor PTEN. Oncogene. 2014;33(42):4997-5005. Epub 2013/10/22. doi: 10.1038/onc.2013.437. PubMed PMID: 24141775; PMCID: PMC3994182.
59. Sidonio RF, Jr., Pipe SW, Callaghan MU, Valentino LA, Monahan PE, Croteau SE. Discussing investigational AAV gene therapy with hemophilia patients: A guide. Blood Rev. 2021;47:100759. Epub 2020/11/14. doi: 10.1016/j.blre.2020.100759. PubMed PMID: 33183859.
60. Kaiser J. How safe is a popular gene therapy vector? Science. 2020;367(6474):131. Epub 2020/01/11. doi: 10.1126/science.367.6474.131. PubMed PMID: 31919200.
61. Fong S, Handyside B, Sihn CR, Liu S, Zhang L, Xie L, Murphy R, Galicia N, Yates B, Minto WC, Vitelli C, Harmon D, Ru Y, Yu GK, Escher C, Vowinckel J, Woloszynek J, Akeefe H, Mahimkar R, Bullens S, Bunting S. Induction of ER Stress by an AAV5 BDD FVIII Construct Is Dependent on the Strength of the Hepatic-Specific Promoter. Mol Ther Methods Clin Dev. 2020;18:620-30. Epub 2020/08/11. doi: 10.1016/j.omtm.2020.07.005. PubMed PMID: 32775496; PMCID: PMC7397702.
62. Karin M, Cao Y, Greten FR, Li ZW. NF-kappaB in cancer: from innocent bystander to major culprit. Nat Rev Cancer. 2002;2(4):301-10. Epub 2002/05/11. doi: 10.1038/nrc780. PubMed PMID: 12001991.
63. Rutkowski DT, Wu J, Back SH, Callaghan MU, Ferris SP, Iqbal J, Clark R, Miao H, Hassler JR, Fornek J, Katze MG, Hussain MM, Song B, Swathirajan J, Wang J, Yau GD, Kaufman RJ. UPR pathways combine to prevent hepatic steatosis caused by ER stress-mediated suppression of transcriptional master regulators. Dev Cell. 2008;15(6):829-40. Epub 2008/12/17. doi: 10.1016/j.devcel.2008.10.015. PubMed PMID: 19081072; PMCID: PMC2923556.
64. Zhang K, Shen X, Wu J, Sakaki K, Saunders T, Rutkowski DT, Back SH, Kaufman RJ. Endoplasmic reticulum stress activates cleavage of CREBH to induce a systemic inflammatory response. Cell. 2006;124(3):587-99. Epub 2006/02/14. doi: 10.1016/j.cell.2005.11.040. PubMed PMID: 16469704.
65. de Jong YP, Herzog RW. Liver gene therapy and hepatocellular carcinoma: A complex web. Mol Ther. 2021;29(4):1353-4. Epub 2021/03/21. doi: 10.1016/j.ymthe.2021.03.009. PubMed PMID: 33743193; PMCID: PMC8058499.
66. Febbraio MA, Reibe S, Shalapour S, Ooi GJ, Watt MJ, Karin M. Preclinical Models for Studying NASH-Driven HCC: How Useful Are They? Cell Metab. 2019;29(1):18-26. Epub

2018/11/20. doi: 10.1016/j.cmet.2018.10.012. PubMed PMID: 30449681; PMCID: PMC6326872.
67. Kim JY, He F, Karin M. From Liver Fat to Cancer: Perils of the Western Diet. Cancers (Basel). 2021;13(5). Epub 2021/04/04. doi: 10.3390/cancers13051095. PubMed PMID: 33806428; PMCID: PMC7961422.
68. Dalwadi DA, Torrens L, Abril-Fornaguera J, Pinyol R, Willoughby C, Posey J, Llovet JM, Lanciault C, Russell DW, Grompe M, Naugler WE. Liver Injury Increases the Incidence of HCC following AAV Gene Therapy in Mice. Mol Ther. 2021;29(2):680-90. Epub 2021/02/09. doi: 10.1016/j.ymthe.2020.10.018. PubMed PMID: 33554867; PMCID: PMC7854305.
69. Lange AM, Altynova ES, Nguyen GN, Sabatino DE. Overexpression of factor VIII after AAV delivery is transiently associated with cellular stress in hemophilia A mice. Mol Ther Methods Clin Dev. 2016;3:16064. Epub 2016/10/16. doi: 10.1038/mtm.2016.64. PubMed PMID: 27738645; PMCID: PMC5040173.
70. Zolotukhin I, Markusic DM, Palaschak B, Hoffman BE, Srikanthan MA, Herzog RW. Potential for cellular stress response to hepatic factor VIII expression from AAV vector. Mol Ther Methods Clin Dev. 2016;3:16063. Epub 2016/10/16. doi: 10.1038/mtm.2016.63. PubMed PMID: 27738644; PMCID: PMC5040172.
71. Brunt EM. Histopathologic features of hepatocellular carcinoma. Clin Liver Dis (Hoboken). 2012;1(6):194-9. Epub 2013/01/23. doi: 10.1002/cld.98. PubMed PMID: 31186886; PMCID: PMC6499305.
72. Coston WM, Loera S, Lau SK, Ishizawa S, Jiang Z, Wu CL, Yen Y, Weiss LM, Chu PG. Distinction of hepatocellular carcinoma from benign hepatic mimickers using Glypican-3 and CD34 immunohistochemistry. Am J Surg Pathol. 2008;32(3):433-44. Epub 2008/02/28. doi: 10.1097/PAS.0b013e318158142f. PubMed PMID: 18300806.
73. Garcia-Buitrago MT. Beta-Catenin Staining of Hepatocellular Adenomas. Gastroenterol Hepatol (N Y). 2017;13(12):740-3. Epub 2018/01/18. PubMed PMID: 29339950; PMCID: PMC5763560.
74. Flanagan BF, Dalchau R, Allen AK, Daar AS, Fabre JW. Chemical composition and tissue distribution of the human CDw44 glycoprotein. Immunology. 1989;67(2):167-75. Epub 1989/06/01. PubMed PMID: 2666306; PMCID: PMC1385252.
75. Ji J, Wang XW. Clinical implications of cancer stem cell biology in hepatocellular carcinoma. Semin Oncol. 2012;39(4):461-72. Epub 2012/08/01. doi: 10.1053/j.seminoncol.2012.05.011. PubMed PMID: 22846863; PMCID: PMC3409471.
76. Basakran NS. CD44 as a potential diagnostic tumor marker. Saudi Med J. 2015;36(3):273-9. Epub 2015/03/05. doi: 10.15537/smj.2015.3.9622. PubMed PMID: 25737167; PMCID: PMC4381009.

Figure 1

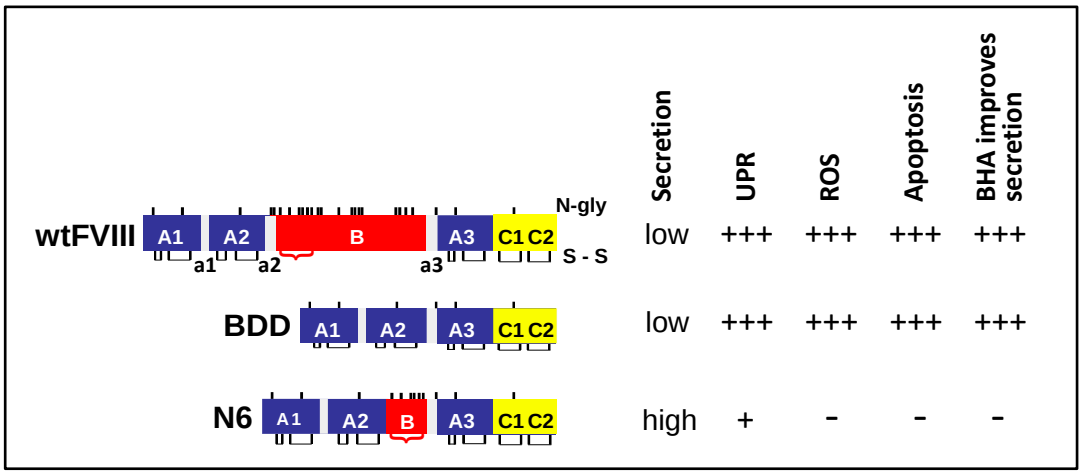

Figure 2

A FVIII aggregates induced by glucose depletion begin to resolve at 1 hr following glucose repletion

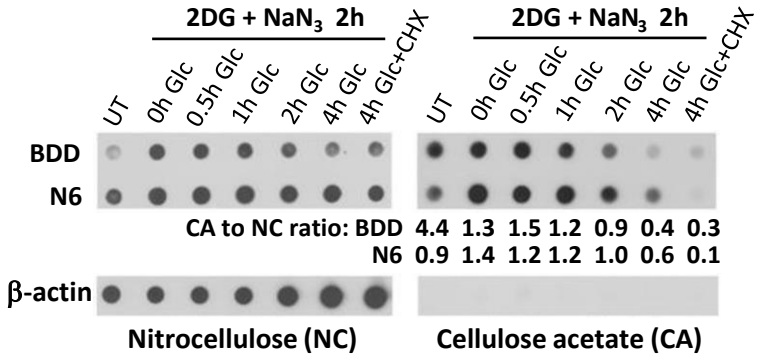

B Reversible retention and secretion of active FVIII in CHO cells

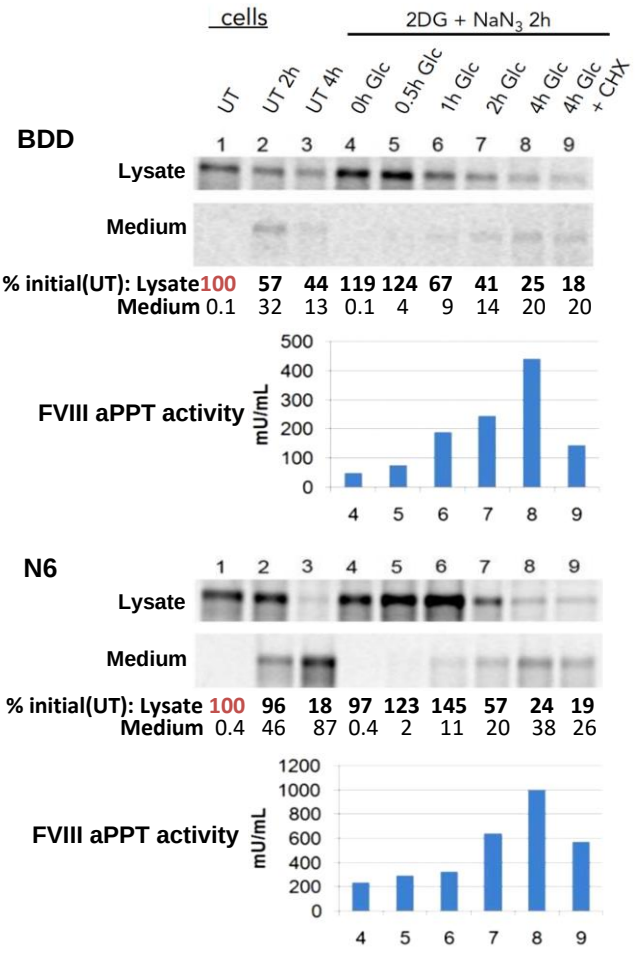

Figure 3

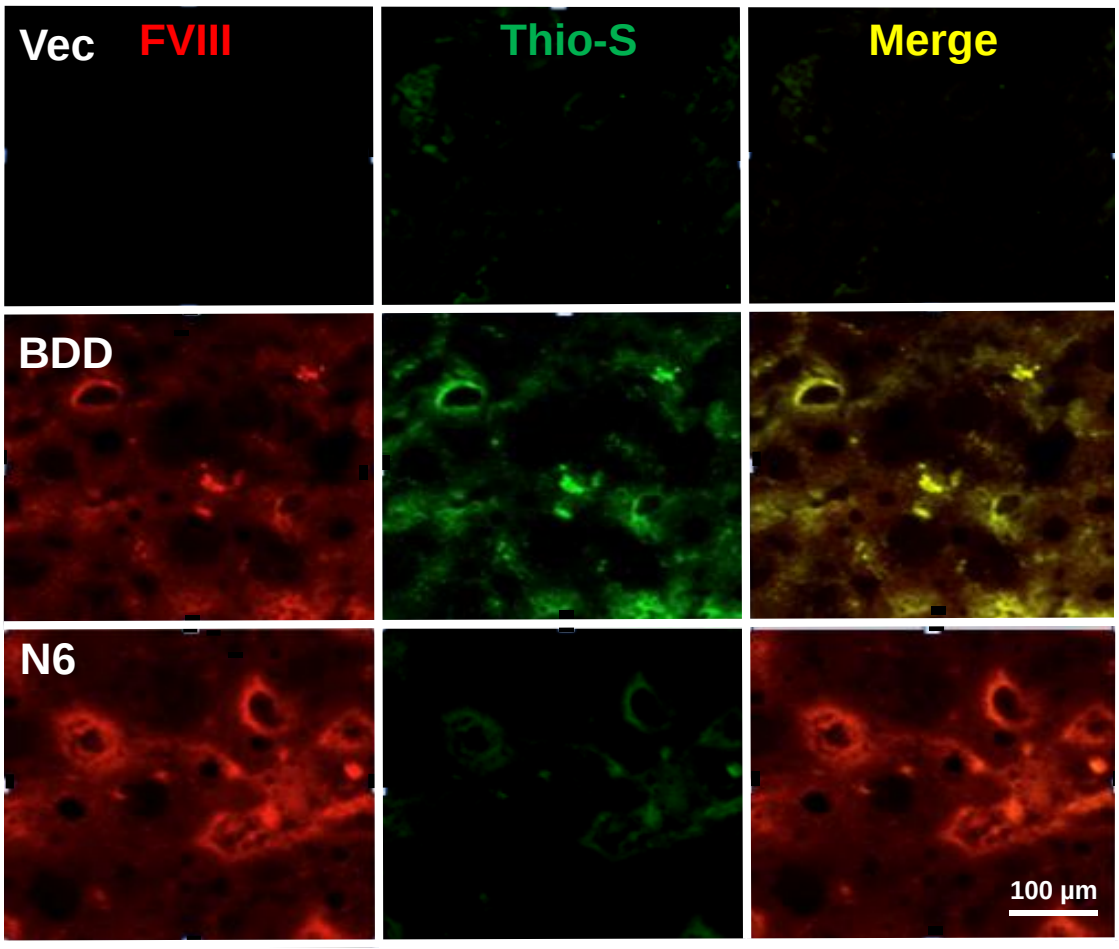

Figure 4

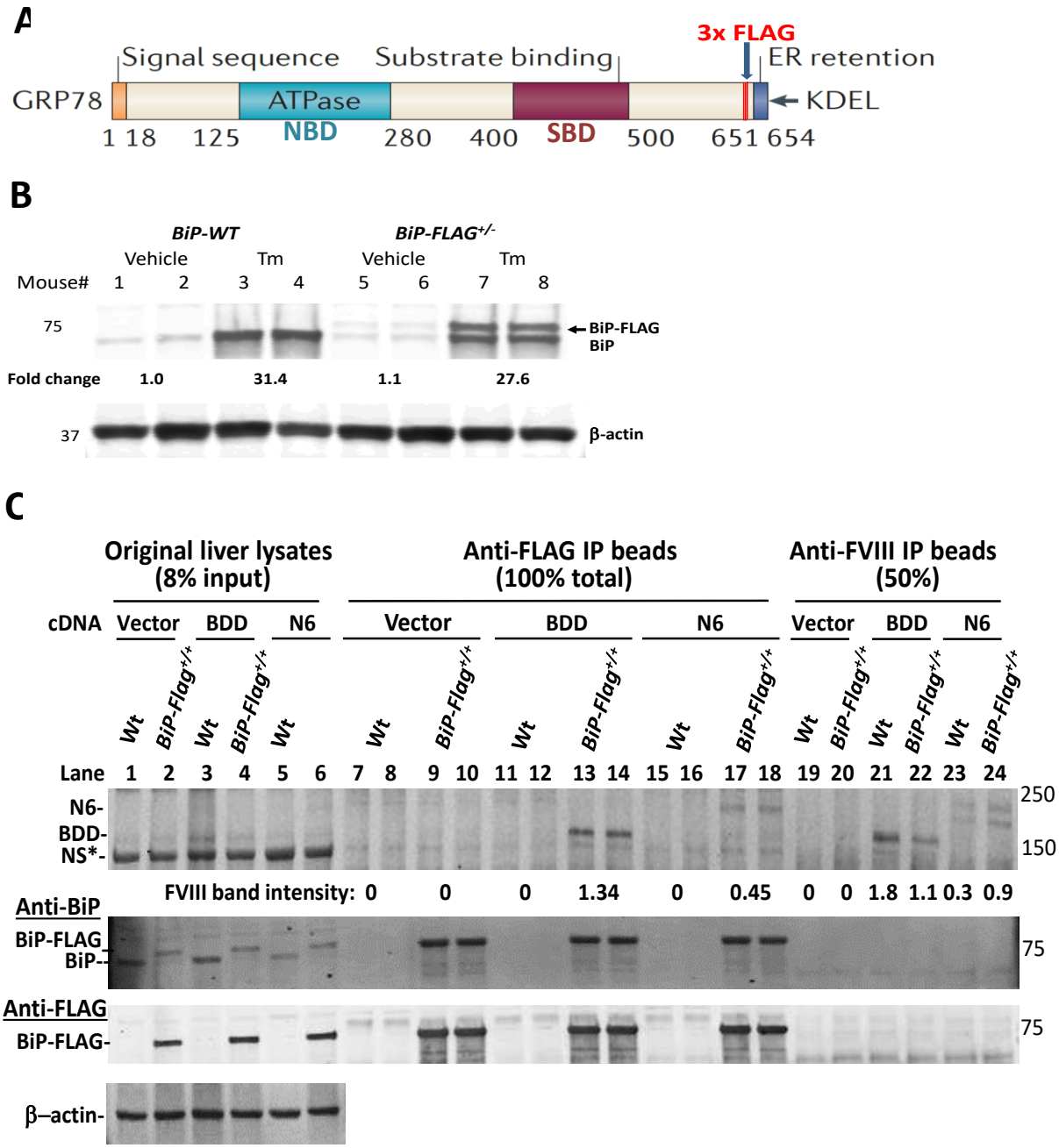

Figure 5

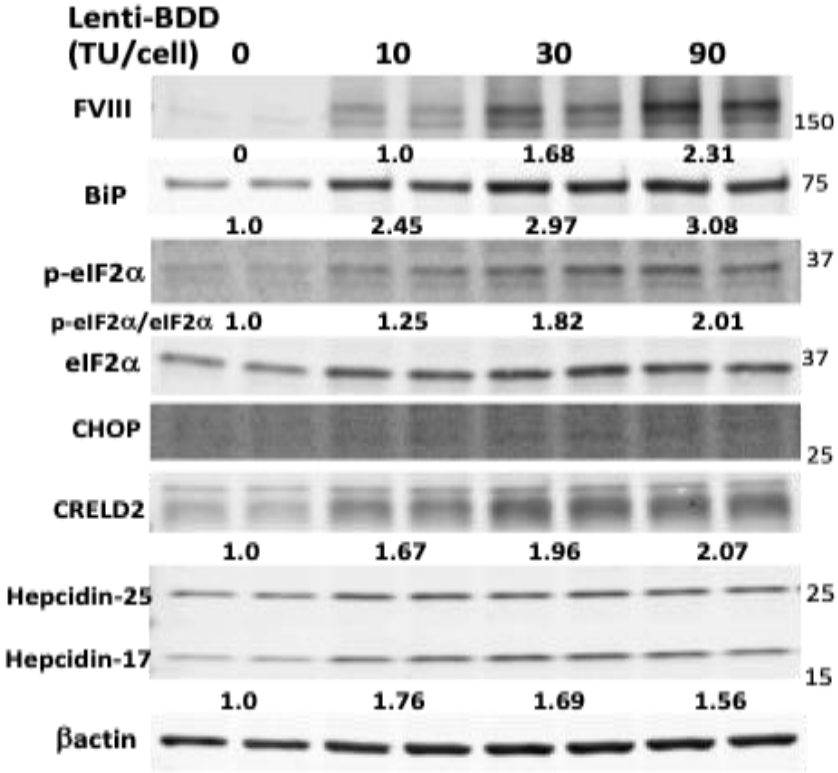

Figure 6

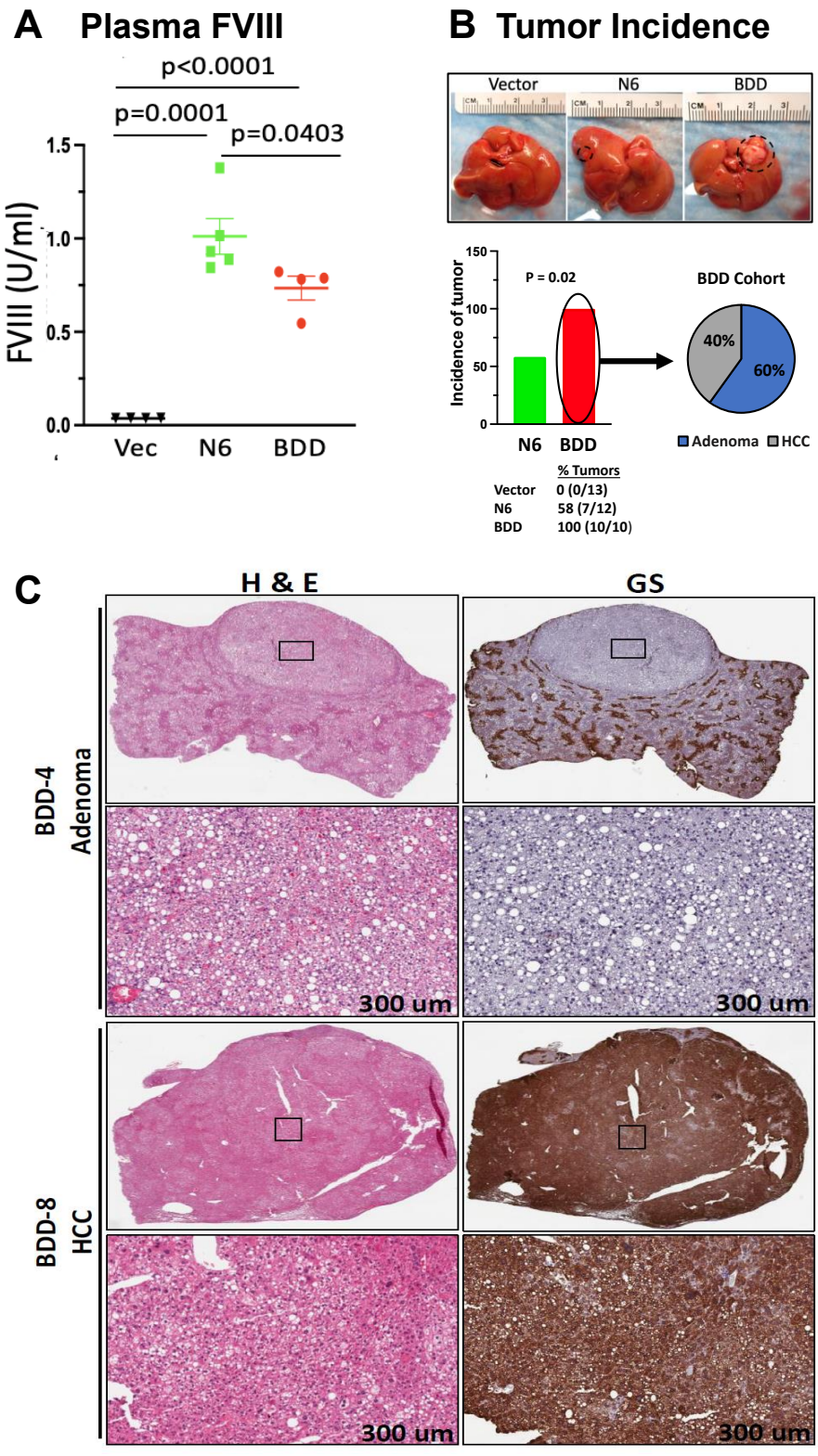

Figure 7

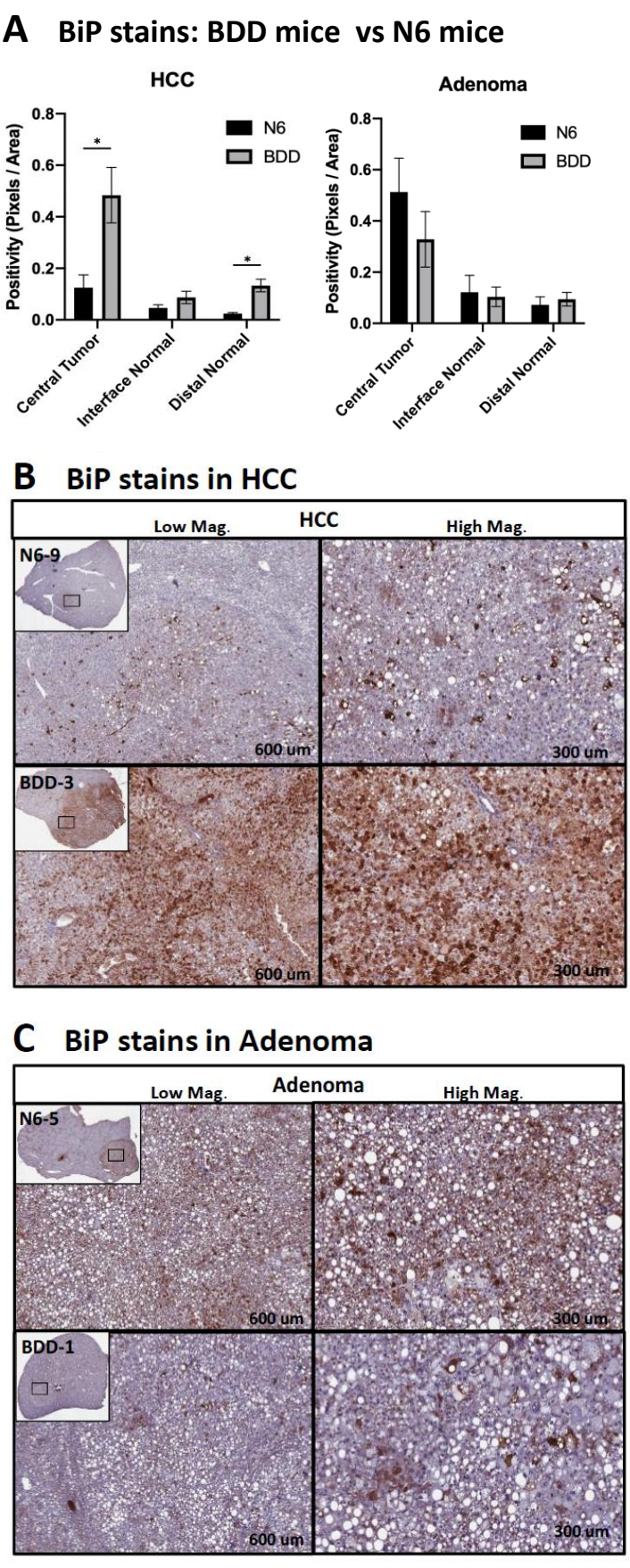

Figure S1

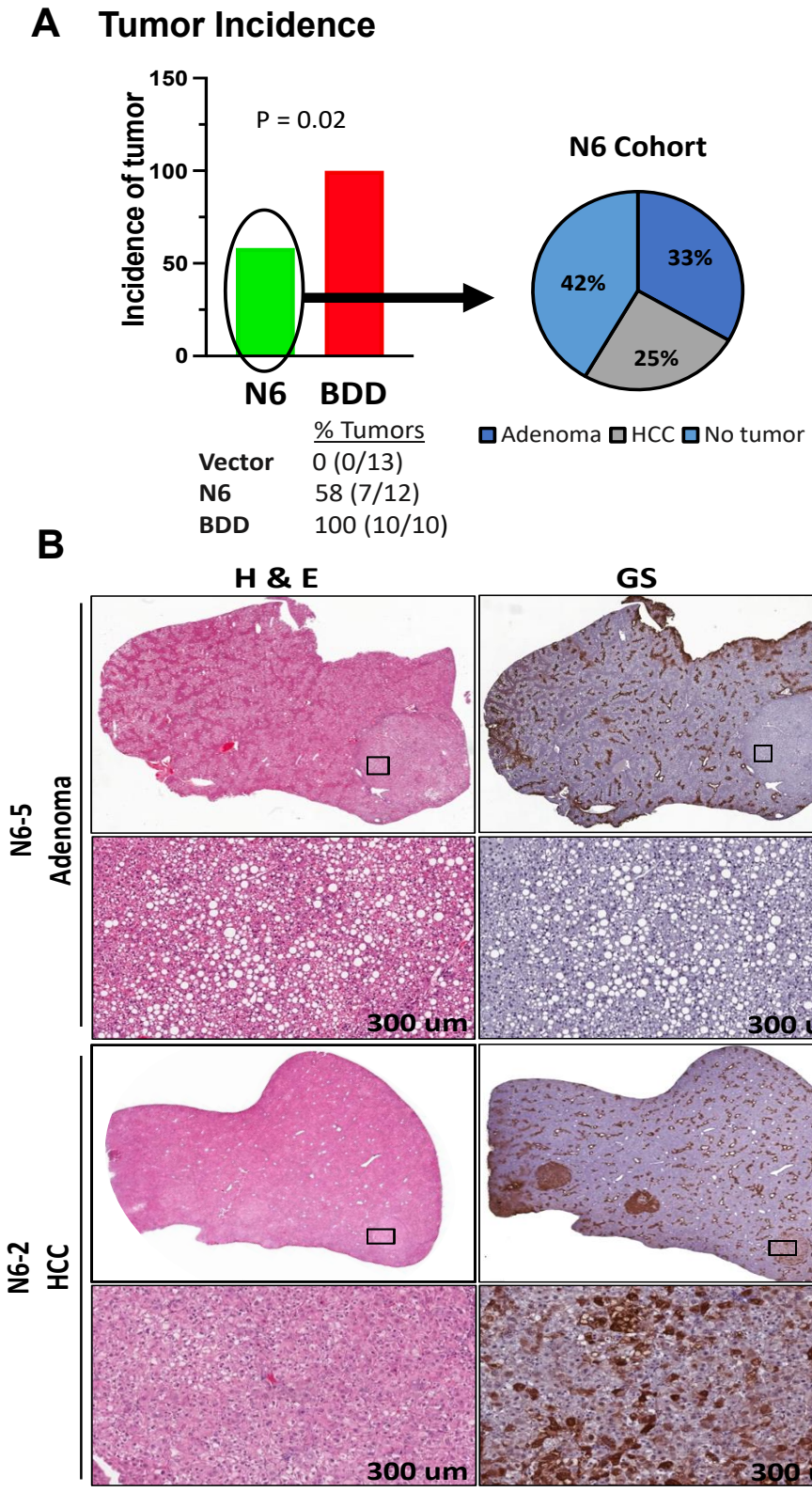

Figure S2

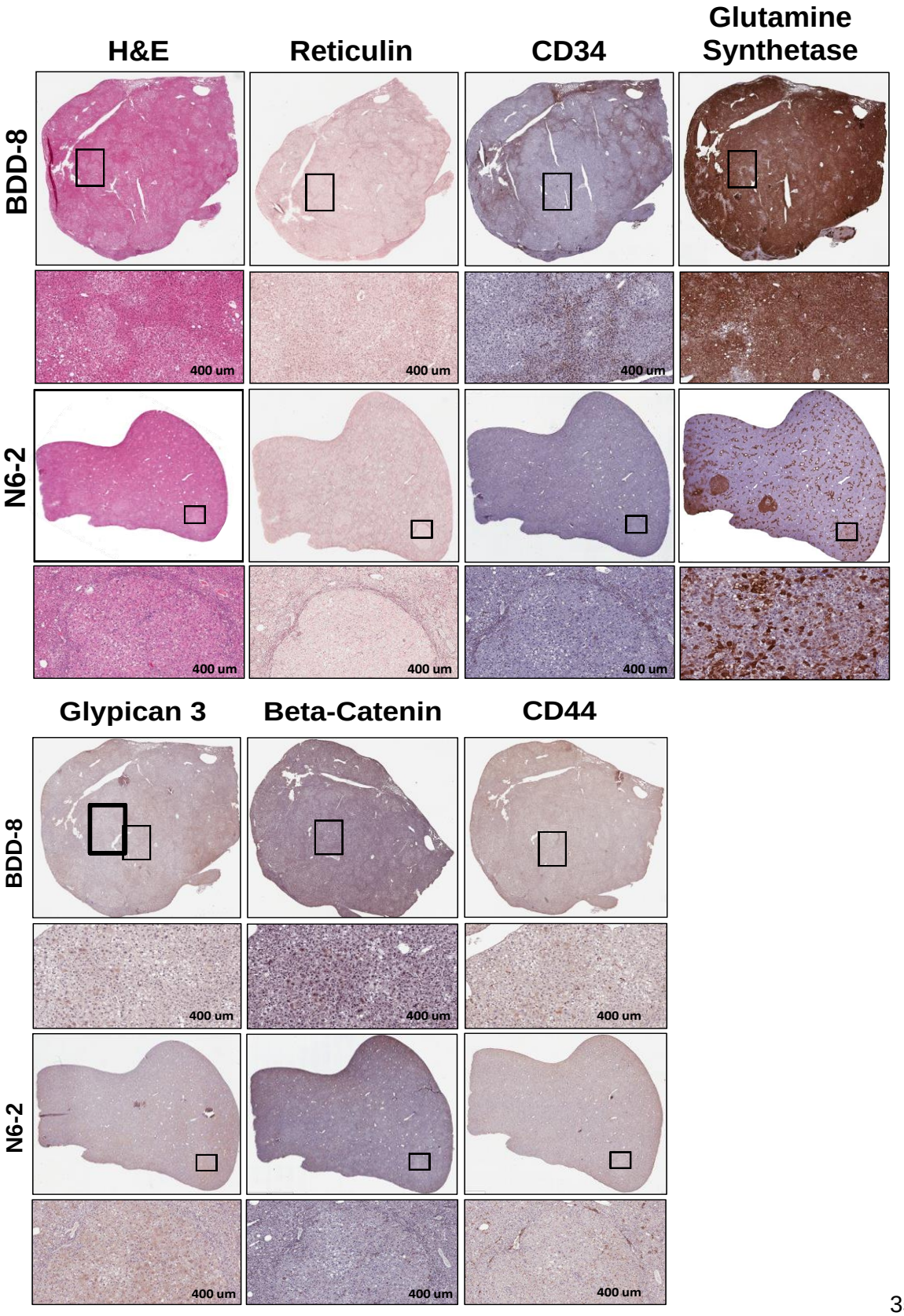

Figure S3

	BIP
BDD-10	**The tumor showed patchy intense staining (3+).** No stain in the background liver.
BDD-9	**The tumor showed patchy intense staining (2+).** Background liver also showed patchy intense staining.
BDD-8	The tumor showed patchy intense staining (2+)
BDD-7	The poorly demarcated nodule showed essentially no stain. Same as background liver.
BDD-6	**Tumor showed much stronger (3+) staining intensity tan background liver**
BDD-5	**8% of the tumor showed stronger (2+) staining intensity than background liver**
BDD-4	**Tumor showed stronger (2+) staining intensity than background liver**
BDD-3	**Tumor showed much stronger (3+) staining intensity tan background liver**
BDD-2	The infiltrating lymph plasmacytes showed strong staining. Lesioinal hepatocytes showed similar staining intensity with background liver.
BDD-1	Lesion showed slightly less staining intensity than background liver. Within the lesion, small patchy areas showed stronger staining.

	BIP
N6-12	No tumor, no stain.
N6-11	**Tumor showed much stronger (3+) staining intensity than background liver.** Background liver showed some patch staining.
N6-10	
N6-9	**Tumor showed patchy much stronger (2+) staining intensity than background liver**
N6-8	**Tumor showed much stronger (2+) staining intensity than background liver**
N6-7	One poorly demarcated nodular area showed much stronger staining than background liver (3+)
N6-6	Lesion no satin, same as background liver.
N6-5	**Tumor showed much stronger (3+) staining intensity than background liver**
N6-4	No tumor, patchy background staining (2+).
N6-3	No tumor, no stain
N6-2	The lesion showed no stain, same as background liver.
N6-1	**Tumor showed much stronger (2-3+) staining intensity than background liver**

Table S1. Immunohistochemistry characterization of the BDD cohort samples.

	H&E	Glutamine synthetase	CD34	Reticulin	B-catenin	CD44	Glypican 3	AFP
BDD-10	Steatosis involves about 30% liver parenchyma with mild steatohepatitis. There is one large well-defined lesion with 75% steatosis, inflammation and ductular proliferation favor **liver cell adenoma**. Focal nodular hyperplasia is in the differential.	Tumor completely negative	Patchy strong positive in the center of the lesion	Patchy loss of reticulin network.	Mostly negative (80%) Focal (10%) patchy cytoplasmic and nuclear positivity Other 10% positive cells are inflammatory cells	Some sinusoidal lymphocytes positive, all lesional hepatocytes negative	Lesion negative.	Background no obvious stain. Tumor even more pale. Consider negative.
BDD-9	Steatosis involves about 5% liver parenchyma with no steatohepatitis. Occasional portal tract has dense lymphplasmacytic aggregate. A well demarcated nodule with mild cytological atypia, **early HCC**.	The tumor stained completely positive, may indicate malignant	Lesion negative	Tumor nearly completely loss of reticulin network, favor malignant	Lesion negative	Lesion negative	Focal weak positivity (1+) especially in cells showing nuclear atypia	Heavy background, Tumor non-steatotic cells showed stronger staining than the background liver.
BDD-8	Steatosis involves about 5% liver parenchyma with no steatohepatitis. A tumor lesion with poorly defined borders and cytological atypia, could be an **early HCC**.	Entire slide stained positive, patchy pale focus, may indicate malignant	Lesion mostly negative, at one end, Patchy strong positivity	Reticulin is lost in 80% of the lesion	Nuclear positivity present	Lesion negative	Lesion showed patchy positivity 1+.	Heavy background, tumor showed patchy strong positivity.
BDD-7	Steatosis involves about 55% liver parenchyma with mild steatohepatitis. There is a **small poorly demarcated** nodule at the center of the slide.	Very small poorly developed lesion area, stained negative	Lesional area positive, periphery, extend to the center	Lesional area showed diminished reticulin and focal loss.	Lesion negative	Some sinusoidal lymphocytes positive, all lesional and non-lesional hepatocytes negative	Lesion completely negative	Heavy background. The poorly demarcated nodule showed essentially no stain.
BDD-6	Steatosis involves about 5% liver parenchyma with no steatohepatitis. There is a large lesion with significant ballooning, inflammation, nodularity and focal ductular proliferation. Favor **liver cell adenoma** inflammatory subtype.	Lesion negative Favor adenoma, ruled out FNH	Overall, the lesion is negative	Lesion showed diminished reticulin and focal loss.	Lesion negative	Some sinusoidal lymphocytes positive, all lesional and non-lesional hepatocytes negative	Lesion completely negative	Heavy background. Tumor showed patch weak positivity.
BDD-5	Steatosis involves about 30% liver parenchyma with mild steatohepatitis. There is one large well-defined lesion with 100% steatosis, and bland cytology. **Favor liver cell adenoma**. Above that, a small round nodule also present.	Upper small nodule negative. Lesion middle area negative Lesion lower area patchy positive normal liver pattern.	Positive mostly at the periphery of the upper small round nodule. Lower large lesion negative	Upper small nodule completely lost reticulin. Remaining lesion showed diminished reticulin.	Lesion negative	Upper small nodule negative. The larger nodule showed focal hepatocyte 1+ membranous positivity.	Upper small nodule negative. Large nodule mostly negative. At the lower part, focal positivity at the edge with no corresponding HCC morphology	Heavy background, Tumor showed less staining due to steatosis. Non steatotic area of the tumor show similar staining intensity with the background liver.
BDD-4	Steatosis involves about 30% liver parenchyma with mild steatohepatitis. There is one large well-defined lesion with 40% steatosis, and bland cytology, **favor liver cell adenoma.**	Lesion negative	Lesion negative	Reticulin present in at least 50% of the lesion. Diminished reticulin network.	Lesion negative	Lesion negative	Lesion negative	Heavy background, tumor essentially negative
BDD-3	Steatosis involves about 45% liver parenchyma with mild steatohepatitis. There is one focus of **well differentiated HCC** arising from a large liver cell adenoma.	Lesion negative	With the nodule, a strong positive area "nodule in nodule) support HCC arising from an adenoma	Approximately 65% of lesion showed loss of reticulin Diminished reticulin network. The area with no reticulin correspond to the malignant looking area in HE	Some cytoplasmic stain see especially in the "HCC" area, no obvious nucleus stain	Some sinusoidal lymphocytes positive, all lesional and non-lesional hepatocytes negative	Lesion negative	Heavy background. Tumor overall less staining than the background liver, patch weak stains.
BDD-2	Steatosis involves about 5% liver parenchyma with no steatohepatitis. The is a **liver cell adenoma** with dense lymphplasmacytic aggregates mimicking lymphoma.	Lesion negative, normal liver distribution	Lesion negative	Difficult to assess due to the inflammatory cell aggregate. Appears some reduction of reticulin in the lesional area.	Lesion negative	Dense lymphoid aggregates positive, all lesional and non-lesional hepatocytes negative	Lesion negative	Heavy background, tumor showed a little stronger staining than the background liver
BDD-1	Steatosis involves about 40% liver parenchyma with minimum steatohepatitis. There is a well demarcated lesion with bland cytology **favor liver cell adenoma**.	Lesion negative	Lesion negative	Approximately 75% of lesion showed loss of reticulin Diminished reticulin network.	Lesion negative	Some sinusoidal lymphocytes positive, all lesional and non-lesional hepatocytes negative	Lesion negative	Heavy background, Tumor showed less staining due to steatosis, less steatotic area of the tumor patchy positive areas

Table S2. Immunohistochemistry characterization of the N6 cohort samples.

	H&E	Glutamine synthetase	CD34	Reticulin	Beta-catenin	CD44	Glypican 3	AFP
N6-12	Dense lymphoplasmacytic aggregates seen in 5 portal tracts. Steatosis involves about 45% liver parenchyma with mild steatohepatitis. **No tumor.**	Normal distribution staining	No tumor	Normal staining pattern	No lesion. Cytoplasmic positivity seen in liver cells at the edge of the tissue (edge effect)	negative	Essentially all negative. At one edge, patch 1-2+ staining noted.	No tumor
N6-11	Steatosis involves about 40% liver parenchyma with moderate steatohepatitis. Occasional portal tract has dense lymphplasmacytic aggregate. There is one well-defined lesion with 100% steatosis, **favor a small adenoma.**	The nodule showed no staining	Patchy positivity inside nodule	Entire lesion showed diminished staining	Lesion negative. Some inflammatory cells positive.	Lesion negative	Lesion negative	Heavy background. Lesion showed slightly les staining intensity than background liver.
N6-10	Steatosis involves about 35% liver parenchyma with mild steatohepatitis. Occasional portal tract has dense lymphplasmacytic aggregate. There is one well-defined subcapsular lesion with 80% steatosis and mild cytological atypia, **favor liver cell adenoma.**	Tumor mostly positive	Lesion negative	Lesion cells 1-2 cells thick, normal reticulin	Lesion negative	Lesion negative	Lesion negative	Heavy background, Tumor non-steatotic cells showed similar staining than the background liver.
N6-9	Steatosis involves about 35% liver parenchyma with mild steatohepatitis. Occasional portal tract has dense lymphplasmacytic aggregate. There is one well-defined lesion with dense cellularity and moderate cytological atypia, **favor early HCC.**	Tumor diffuse strong staining	Lesion negative	Diminished reticulin, thick trabeculae, consistent with HCC	Lesion negative	Lesion negative	The lesion showed diffuse faint positivity 1+, better appreciate at low power	**Tumor show much stronger staining intensity than background liver**
N6-8	Steatosis involves about 45% liver parenchyma with mild steatohepatitis. There are two lesions, one is better demarcated than the other. The well-defined lesion has mild cytological atypia, **favor liver cell adenoma.**	The poorly demarcated nodule, no staining, the well demarcated nodule showed patchy staining	The poorly demarcated nodule, showed some intralesionnal positivity, the well demarcated nodule is completely negative	The poorly demarcated nodule completely lost reticulin, favor HCC. The well demarcated nodule reticulin diminished.	The poorly demarcated nodule showed areas of nuclear and cytoplasm positivity. The well demarcated nodule mostly negative with some inflammatory cells positive.	Lesion showed focal positivity 2+, mostly inflammatory cells in sinusoids are positive. Only a few hepatocytes positive.	The lesion showed patchy focal positivity 1-2+	Heavy background. One lesion showed stronger staining than background liver. The other lesion showed similar staining intensity with background liver.
N6-7	Steatosis involves about 20% liver parenchyma with mild steatohepatitis. **No tumor.**	Normal distribution staining. At one edge, a poorly demarcated intensive staining area noted.	No tumor.	Normal staining pattern	No tumor. A focal positive are likely due to staining artefact	Some sinusoidal lymphocytes positive, all hepatocytes negative	Patch 1-2+ staining, especially at one edge where the hepatocyte nuclei appears a bit atypical	Heavy background, no tumor
N6-6	Steatosis involves about 60% liver parenchyma with mild steatohepatitis. Occasional portal tract has dense lymphplasmacytic aggregate. A very small nodular area noted, no obvious cytological atypia. **Could evolve into an adenoma but not there yet.**	Normal distribution staining, a small nodular focus showed lack of staining	A small nodular focus, no stain.	The nodular focus showed slightly diminished reticulin, not obvious	Lesion negative	In addition to the sinusoidal lymphocytes, the lesional hepatocytes showed faint membranous staining 1+	Patchy 1-2+ staining, especially at the nodular focus area.	Lesion non lesion, no difference. Heavy background
N6-5	Steatosis involves about 65% liver parenchyma with mild steatohepatitis. There is one well-defined lesion with 75% steatosis, **favor liver cell adenoma.**	Lesion negative	Lesion negative	Reticulin loss in the lesion area	Lesion negative. At the interface with non-neoplastic liver, focal cytoplasmic positivity noted.	Lesion negative	Very small focal areas in the lesion positive (1-2+). Mostly the lesion negative	Shattered, heavy background. Lesional area looks paler.
N6-4	Steatosis involves about 85% liver parenchyma with mild steatohepatitis. There is a 0.07 cm area with cell ballooning and start forming a nodular appearance. **No definitive tumor.**	Normal distribution staining	Negative	Normal reticulin network	No lesion, staining quality not good, cytoplasmic staining see in patchy areas, probably not real.	All negative	Focal and patchy 2+ staining noted.	No tumor, heavy background.
N6-3	Steatosis involves about 65% liver parenchyma with mild steatohepatitis. **No tumor.**	Normal distribution staining	Negative	Normal reticulin network	No lesion. Cytoplasmic positivity seen in liver cells at the edge of the tissue (edge effect)	All negative	No tumor, all negative	No tumor, some background staining
N6-2	Steatosis involves about 10% liver parenchyma with mild steatohepatitis. Occasional portal tract has dense lymphplasmacytic aggregate. There is one well-defined lesion with obvious cytological atypia and mitoses, **favor early evolving hepatocellular carcinoma.** Two small poorly demarcated nodules with similar degree cytological atypia can also be appreciated.	Showed 3 nodules, all positive	Lesions all Negative. Only one nodule obvious	Reticulin loss in noe nodule. Diminished reticulin in two other nodules.	2 small lesions negative. 1 larger lesion showed focal patchy cytoplasmic positivity	one small lesion negative. The larger well recognized lesion and one small lesion showed 1+ membranous staining on hepatocytes	2 small lesions negative. The larger well recognized lesion positive (1-2+)	One poor demarcated nodule showed stronger staining than the background liver
N6-1	Steatosis involves about 35% liver parenchyma with mild steatohepatitis. Occasional portal tract has dense lymphplasmacytic aggregate. There is one well-defined lesion **well differentiated hepatocellular carcinoma.** Two small poorly demarcated nodules with similar degree cytological atypia can also be appreciated.	Tumor diffusely positive	Strong positivity inside the tumor in two lesions. 3rd one no stain (unable to recognize the nodule)	The large nodule showed areas lost reticulin. Favor malignant.	Lesion strong cytoplasmic positivity, patchy but real	Tumor negative. The dense lymphoid aggregate between two vessels showed 3+ staining.	Entire lesion faint positive 1+. Non-neoplastic liver showed patchy positivity (2+).	Heavy background. Tumor showed patch strong positivity.